744212

A NUMERICAL THERMO-MECHANICAL MODEL FOR THE WELDING AND SUBSEQUENT LOADING OF A FABRICATED STRUCTURE

H. D. HIBBITT and P. V. MARÇAL

N00014-0006/2

D D C
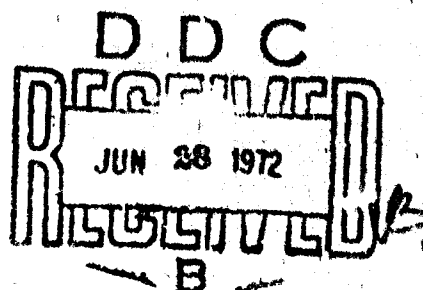
JUN 28 1972

B

March 1972

A Numerical, Thermo-Mechanical Model for the

Welding and Subsequent Loading of a Fabricated Structure[*]

by

Hugh D. Hibbitt[1] and Pedro V. Marcal

Brown University, Providence, R.I. 02912

Ia

DOCUMENT CONTROL DATA - R & D

(Security classification of title, body of abstract and indexing annotation must be entered when the overall report is classified)

1. ORIGINATING ACTIVITY (Corporate author)	2a. REPORT SECURITY CLASSIFICATION
Brown University Division of Engineering Providence, Rhode Island	Unclassified
	2b. GROUP N/A

3. REPORT TITLE

A Numerical, Thermo-Mechanical Model for the Welding and Subsequent Loading of a Fabricated Structure

4. DESCRIPTIVE NOTES *(Type of report and inclusive dates)*

Technical Report

5. AUTHOR(S) *(First name, middle initial, last name)*

Hugh D. Hibbitt and Pedro V. Marcal

6. REPORT DATE	7a. TOTAL NO. OF PAGES	7b. NO. OF REFS
March 1972	34 pages of text	44

8a. CONTRACT OR GRANT NO. N00014-67-A-0191-0006	9a. ORIGINATOR'S REPORT NUMBER(S) N00014-0006/2
b. PROJECT NO.	
c.	9b. OTHER REPORT NO(S) (Any other numbers that may be assigned this report)
d.	

10. DISTRIBUTION STATEMENT

Distribution in whole or in part is permitted for any purpose of the United States Government.

11. SUPPLEMENTARY NOTES	12. SPONSORING MILITARY ACTIVITY
	Naval Ship Research and Development Center

13. ABSTRACT

In this work a numerical model is developed for the welding and subsequent loading of a fabricated structure. The model treats the weld process as a thermo-mechanical problem. A finite element formulation derived from the uncoupled thermal and mechanical energy balances forms the basis of the model. During the development of the thermal model, two significant problems are discussed. One is the material nonlinearity, which manifests itself in the temperature dependence of the thermal properties, and in the fusion problem, where the material phase change is accompanied by a latent heat effect. This latter is modeled by use of a modified specific heat, since the materials of prime concern are alloys which melt over a finite range of temperature, while the former are introduced through periodic re-evaluation of the properties throughout the analysis. The second problem is that of boundary conditions: The deposition of molten bead on the base is modeled by using the intimate contact boundary condition, which is developed into a set of impulse type equations on the finite element model. Since radiation is a dominant cooldown mechanism, this boundary condition is also included. Thus the first part of work develops a non-linear finite element thermal analyzer capable of modeling all of the above effects. This program is then applied to several problems in order to assess its accuracy.

During the second part of the work the mechanical model is described. This is an incremental finite element model in which the basic constitutive descriptions are time independent elastic-plastic behavior with temperature dependent properties, and a creep rate formulation for the time dependent behavior. The development is not based on

(Continued)

Document Control Data - ... & D, DD Form 1473

13. Abstract (cont'd.)

thermodynamic theorie but on direct extension of the classical (isothermal) theories. The model includes f: ;:e strain effects during isothermal loading, so that it may be used in the modelir₁ '' distortion sensitive structures. The integration of the rate equations is discus: ₃ with respect to the introduction of a residual load (total equilibrium) correction; it is shown that such a correction must be introduced very carefully in a completely incremental formulation such as is developed here.

Finally the model ₃ compared with simple bead-on-plate weld experiments, performed with high strength steels., It is found that in one case the experimental approximations are well justified by the finite element results, but there is no agreement with the experimentally measured residual stresses. The suggested explanation for the unique stress patterns observed experimentally is shown to have little effect on the finite element stress predictions, so that it is concluded that the finite element model does not include a significant material behavior in this case. In the second example it is shown that the experimental assumptions were not justified by the results of the present model. In both cases the model predicts the usually expected residual stress patterns. Use of a simple creep formulation is shown to give the same order of residual stress reduction as a result of post weld heat treatment as is measured experimentally.

II

14. KEY WORDS	LINK A		LINK B		LINK C	
	ROLE	WT	ROLE	WT	ROLE	
Structural Analysis						
Welding						
Heat Transfer						
Finite Element Method						

III

Introduction

The welding process is of fundamental technological importance because of its universal use as a fabrication technique. By the very nature of the process, welding subjects parts of the structure to an extremely severe thermal history, so that weld sections are often the critical determinants of the life and working strength of a fabricated structure.

The welding process leaves very large residual stresses in the joint that has been formed, so that weld sections are prone to cracking and subsequent failure under cyclic loading. For these reasons weld fabrication has been the subject of much experimental and analytic investigation, both from the metallurgical and the structural point of view. At present there is much empirical knowledge of the problem, although few analytic models have been developed. The work in this area was surveyed in a 1970 paper by Masubuchi [1]. In that paper are mentioned the numerical models of Tall [2] and Masubuchi, Simmons and Monroe [3], both of which are one-dimensional.

The intention of the present work is to develop a general numerical model of the weld process (from a structural view point) which will be capable of predicting the structurally significant effects of the process on the basis of known behavior of the material and known parameters of the process.

The welding and subsequent loading processes are viewed as a boundary value problem which can be formulated mathematically with knowledge of the material behavior and of the primary boundary conditions (heat input, rate, weld bead deposit rate, cooling conditions, etc.).

Any such modeling of the welding process is different, since the process is highly non-linear because of the wide temperature range covered (from room temperature to a molten state). The finite element method is adopted here because it is readily adapted to non-linear problems, where the non-linearity

occurs due to both geometric and material effects [4-7]. The behavior of the method in such cases is quite well known, and by use of an incremental approach, solutions have been obtained for history dependent material behavior such as might describe a metal alloy during welding [7-8]. The general nature of the method allows the development of general purpose programs covering many geometries and materials [7]. Many such programs exist for linear stress analysis [9] and a growing number exist for non-linear steady-state and dynamic structural and thermal analysis [7], [10]. Because such concepts have been adopted here, the capability developed in this work is not restricted to particular geometries or material behaviors, other than in a very general sense.

The welding and loading processes are now described from the structural viewpoint, with some of the effects which are considered important to a good model emphasized. The structural history divides naturally into two distinct phases:

a) The Welding Process. Here a structure is fabricated by joining its various component parts through a welding technique; that is, fusion of the material around a joint by heating above the melting point, with the addition of molten filler material. This phase is taken to include all events occuring after the start of the initial pre-heating and before the final cooled state is reached.

In the following we have assumed an uncoupling of the thermal and mechanical aspects of the problem. The model adopts a non-thermodynamic, time-independent plasticity theory [11] for most of the analysis. Creep effects are introduced only when essential, such as in the stress relief by post-heating. Then a conventional formulation for creep [12] is employed.

b) The Loading Process. Here the structure is subjected to its working loads, and such effects as geometric instabilities become more important in the

analysis. While this part of the analysis often contains nonlinearities, it falls in a more familiar range of problems (see [4], [5], [6], etc.) and so will not be discussed in detail in the paper.

Theoretical Considerations

Thermal Analysis:

The finite element model for the thermal analysis was developed by uncoupling of the fundamental energy balance postulated in [13]. This required the introduction of uncoupling assumptions, of which the most critical for the present work are the neglect of dimensional changes, and the neglect of cross-coupling between thermal and mechanical work. The reduced thermal energy balance then takes the form

$$\int_V \rho(\hat{r} - \dot{U}(T))dV = \int_S hdS \tag{1}$$

where ρ is the density

$\hat{r}$ is the specific heat flux

S   is the surface area

V   is the volume

h   is the surface heat flux per unit area

and time derivatives are taken with fixed material coordinates.

By introducing the heat flux vector Q_i , we obtain the heat flow rate normal to the plane defined by a unit normal n .

$$Q_i n_i = h \tag{2}$$

By using the Gauss theorem and then introducing a virtual variation, $g(x)$ to apply the Galerkin method we obtain a variational form of the uncoupled energy

balance equation

$$\int_V \rho(\hat{r} - \dot{U})g\,dV + \int_V Q_i \frac{\partial g}{\partial X_i}\,dV = \int_S ghdS \qquad (3)$$

the model is then completed by introducing the Fourier heat law

$$Q_i = -k_{ij}\frac{\partial T}{\partial X_j} \qquad (4)$$

where the conductivity k_{ij} is a function of position X and the temperature T. For all problems considered here, isotropy is assumed:

$$k_{ij} = \delta_{ij}\,k \qquad (5)$$

The rate of change of internal energy is now written in terms of c, the instantaneous rate of change of internal energy with temperature.

$$\dot{U} = c(T, X_i)\dot{T} \qquad (6)$$

Note that c is the instantaneous specific heat except where fusion is occurring, when c also includes latent heat effects. Substituting (4) and (6) in (3) we obtain the final variational form of the uncoupled thermal model as

$$\int_V g\,\hat{r}\,dV - \int_S ghdS = \int_V g\,c\dot{T}dV + \int \frac{\partial g}{\partial X_i}k_{ij}\frac{\partial T}{\partial X_j}\,dV \qquad (7)$$

The finite element form of this equation is then obtained by restricting g to the same functional form as the description of temperature variation in an element.

In the usual finite element procedure we define the temperature T at a point in the element by an interpolation function

$$T = R^N T^N \tag{8}$$

where $R(X_i)$ is the interpolation function and N is a nodal index on which the summation convention is implied.

The virtual variation g is then given by

$$g = R^M g^M \tag{9}$$

Substituting (9) in (7), making appropriate summation over elements and choosing orthogonal variations of the g^M, we obtain

$$\sum_{elements} \int_V (R^M \rho c R^N) dV \, \dot{T}^N = \sum_{elements} \left| \int_V R^M \rho r dV - \int_S R^M h dS - \int (\frac{\partial R^M}{\partial X_i} k_{ij} \frac{\partial R^N}{\partial X_j}) dV T^N \right| \tag{10}$$

which may be written

$$M^{MN} \dot{T}^N = B^M - H^M - K^{MN} T^N \tag{11}$$

with the coefficients referred to as follows:

    M is the internal heat matrix

    B is the consistantly distributed body flux

    H is the consistantly distributed heat flux

    K is the conductivity matrix.

This is the same result for linear problems as that obtained in [14] and [15] where the derivation begins from the diffuser equation or some equivalent statement. The time integration of the numerical model of the uncoupled thermal problem was achieved by using the modified Crank-Nicholson operator due to Wilson and Nickell [14]. This scheme has the advantage of simplicity and worked well for the examples tested. It is also unconditionally stable for linear problems [17]. Both the vectors and matrices are, in general, functions of temperature.

For economy in computing the matrices M and K are not recomputed after
every time step but only as frequently as judged necessary.

Note on Modeling of Physical Phenomena Accompanying Welding

The physical phenomena and boundary conditions accompanying the welding
process are discussed in t is section. Particular attention is given to the
numerical procedures developed to account for the thermal phenomena.

a) Phase Change and Latent Heat. Most workers [18-22] have assumed that the
phase change takes place at some specific temperature T_o . While such models
are of great value for materials exhibiting a single phase change temperature
(such as a pure element or eutectic alloy), Weiner has pointed out [23] that
rather different assumptions are necessary for general alloys which change phase
over a finite temperature range. Following Weiner, we adopt a uniform release
of the latent heat over the range of temperature of phase change. This requires
the location of two distinct discontinuity interfaces (solidus and liquidus) and
the application of an increased 'specific heat' to simulate the latent heat in
the interface region.

b) Prescribed External Heat Flow, h, r. In most cases of electric arc welding,
the resistive heating will be negligible compared to the surface heating from
the arc, so that the body flux r will usually be assumed to be zero. The
external flux h is assumed to be completely known as a function of position
and time. The flux h is the most critical parameter in a welding analysis and
in principle may be obtained as a function of welding parameters. In the present
analysis some very simple assumptions are made. Later suggestions are offered
for improving this part of the modeling.

c) Surface Heat Loss as a Function of Surface Temperature. This is an important
boundary condition which determines much of the intermediate and long term be-
havior of the model. We have used simultaneously the linear Newton convective

cooling and the quartic Stefan-Boltzmann law. The former dominates at temperatures close to ambient while the latter becomes a major factor at the higher temperatures around the melting range.

d) Addition of Molten Filler Material to the Base Metal. Most commonly in welding practice the addition of filler takes place smoothly at a finite rate. In the approximate numerical model developed here, this continuous addition of fill was modeled as a step-wise addition of finite volumes of filler (several elements per step) in infinitesimal time so that an 'intimate contact' problem is created in the form of an impulsive boundary condition extending over finite surfaces. After finite element discretization, the elements of surfaces being brought instantaneously into intimate contact are taken to be the surfaces of elements of the mesh, so that the weld deposition process is modeled as a series of steps in each of which a finite amount of weld filler (corresponding to at least one finite element) is added to the structure in a time interval which is small compared to the time scale of the overall problem. The interface surfaces on both filler and base metal take on the same temperature in that same short interval. Because of the reduced time scale the heat flux across the surfaces dominates this part of the thermal problem and we obtain an impulse type equation from (11)

$$H^{MN}\dot{T}^{N}\Delta t = -H^{M}\Delta t \tag{12}$$

where H^{M} is zero for all but the two surfaces S^{A} and S^{B} brought into intimate contact. The heat flux balance is simply

$$H^{A} = -H^{B} \tag{13}$$

and since the temperatures of corresponding points must be the same immediately after contact, we have a linear relation between nodal temperatures

$$(T^- + \Delta T)^A = S^{AB}(T^- + \Delta T)^B \qquad (15)$$

where the $^-$ superscript indicates quantities prior to contact, and S^{AB} is a linear constraint matrix. Equation (14) is a non-homogeneous constraint condition and is implemented by a generalization of the tying procedures described in [24] by the elimination of dependent unknowns and equations.

f) Location of the Solidus and Liquidus Surfaces. In the model developed above for fusion problems, there are two discontinuity surfaces associated with the solid/liquid phase change. The assumption has been made that the 'latent heat' or energy required for phase change is absorbed uniformly during the temperature change from solidus to liquidus. In the present work the main concern is steel, for which typical values are:

Specific heat outside the melting range ~ .15 BThU/lb°F

Solidus ~ 2600°F, Liquidus ~ 2700°F

'Latent heat' ~ 118.6 BThU/lb. (excluding specific heat)

so that during the phase change the internal energy rate is

$$(.15 + \frac{118.6}{100}) \sim 1.34 \text{ BThU/lb°F}$$

Clearly the discontinuities are large, and as the melting range decrease they become extreme. Because of these severe discontinuities it is not ob how to develop a good model within the conventional finite element approximation. For a finite element model developed with temperature as the dependent variable (such as that used here), continuity of spatial derivatives of temperature is imposed at least within elements and possibly also between them. This is, of course, improper for the latent heat problem.

Because mechanical resistance is absent in the liquid phase and is extremely low in the temperature range close to the melting phase, the primary goal

is to maintain a proper local energy balance during the fusion part of the history. A mean weighted specific heat was calculated for each element by inter-polating for the solidus and liquidus boundary before and after a time interval of integration. It was found that the discontinuities were better modeled by a fine mesh of low order elements because of the discontinuous temperature gradients.

Mechanical Description

In this project we have made use of the small strain large displacement theory [4] of incremental finite element analysis, as derived as a special case of the large strain, large displacement theory by Hibbitt, Rice and Marcal [25]. Much effort has been devoted to the practical application and development of controls for the application of [4]. In order to discuss these procedures we use as a point of departure the incremental stiffness equations written in rate form which also makes use of a linearized incremental stress-strain relation $D_{ijk\ell}$. Because of the displacement assumption, the stress rates are obtained as a linear combination of the nodal displacement rates:

$$\dot{T}_{ij} = D_{ijk\ell} \left(\frac{\partial R^N_{km}}{\partial X_\ell} + \frac{\partial R^M_{pq}}{\partial X_k} \frac{\partial R^N_{pm}}{\partial X_\ell} \bar{u}^M_q \right) \dot{\bar{u}}^N_m + \dot{H}_{ij}(T) \tag{16}$$

where $\bar{u}$ denotes nodal displacements. The additional term $\dot{H}_{ij}(T)$ accounts for the explicit temperature dependence of the stress rate caused by thermal expansion and temperature variation of material properties (Young's modulus, Poisson's ratio and yield stress).

The incremental stiffness equation is given by

$$\dot{\bar{P}}^N_\ell + \bar{P}^N_\ell = \left(k^{(0)NQ}_{\ell r} + k^{(1)NQ}_{\ell r} + k^{(2)NQ}_{\ell r} - \bar{Q}^{NQ}_{\ell r} \right) \dot{\bar{u}}^Q_r \tag{17}$$

where

$$k_{\ell r}^{(0)NQ} = \sum_{\text{elements}} \int_{V^o} \frac{\partial R_{i\ell}^N}{\partial X_j} D_{ijkp} \frac{\partial R_{kr}^Q}{\partial X_p} dv^o$$

is the usual small displacement stiffness matrix,

$$k_{\ell r}^{(1)NQ} = \sum_{\text{elements}} \int_{V^o} \dot{T}_{ij} \frac{\partial R_{k\ell}^N}{\partial X_i} \frac{\partial R_{kr}^Q}{\partial X_j} dv^o$$

is the initial stress stiffness matrix,

$$k_{\ell r}^{(2)NQ} = \sum_{\text{elements}} \int_{V^o} D_{ijkp} [\bar{u}_q^M (\frac{\partial R_{tq}^M}{\partial X_k} \frac{\partial R_{tr}^Q}{\partial X_p} \frac{\partial R_{i\ell}^N}{\partial X_j}$$

$$+ \frac{\partial R_{kr}^Q}{\partial X_p} \frac{\partial R_{tq}^M}{\partial X_j} \frac{\partial R_{t\ell}^N}{\partial X_i}) + \bar{u}_q^M \bar{u}_f^P \frac{\partial R_{tq}^M}{\partial X_k} \frac{\partial R_{tr}^Q}{\partial X_p} \frac{\partial R_{g\ell}^N}{\partial X_i} \frac{\partial R_{gf}^P}{\partial X_i}] dv^o$$

is the initial displacement stiffness matrix

$\bar{Q}_{\ell r}^{NQ}$ is the load stiffness matrix, and

$$\dot{P}_\ell^N = - \sum_{\text{elements}} \int_{V^o} \dot{H}_{ij} (\frac{\partial R_{i\ell}^N}{\partial X_j} + \frac{\partial R_{k\ell}^N}{\partial X_i} \frac{\partial R_{km}^M}{\partial X_j} \bar{u}_m^M) dv^o$$

is the thermal load vector.

Equation (17) is linear in the nodal displacement rates and may be solved for them. It should be noted that the load stiffness matrix is not symmetric. Since it is customary to take advantage of symmetry in solving structural stiffness equations, it is often more convenient, and usually adequate, to move the term $\bar{Q}_r^{NQ} \dot{u}_r^Q$ to the right-hand side and treat it as a load, by iterating for the $\dot{u}^Q$ if necessary.

We shall now discuss the integration of the rate equations. Probably the most common integration scheme adopted has been the Euler method, which steps out the solution from the first derivative term in a Taylor expansion, the zeroth term being dropped. This method is the most straightforward -- in effect all that is necessary is to replace the rates in equation (17) by the corresponding increments (e.g., $\dot{u} \rightarrow \Delta u$). The method has been shown to give accurate solutions for many problems, [7, 26, 27, 28]. The present work requires the solution to be propagated over many steps, because the thermal history is so complex; in fact, the solutions necessarily involve an order of magnitude more steps than are used in the examples of the above mentioned references. For this reason it is valuable to look at the application of the simple residual load correction discussed in [29-31]. This correction is the topic of the remainder of this section. The correction consists in retaining the zeroth term in the Taylor expansion as a measure of the out-of-equilibrium forces. It will be shown that when such a correction in included with a rate formulation such as (17) above, the strain must be accumulated exactly and not merely by summation of the truncated increments, otherwise the residual load correction may introduce further error.

For the purposes of this discussion it is convenient to introduce some simplified notation. The finite element equilibrium equation is written as

$$\underline{P} = \underline{I}$$

where

$$\underline{I} = \sum_{\text{elements}} \int_{V^o} \underline{B}^T \underline{\sigma}\ dV^o \qquad (18)$$

and $\underline{B}$ is the interpolation function, $\underline{\sigma}$ are stresses, $\underline{P}$ are the consistent nodal forces.

The simple Euler integration is obtained from (17) as

$$\Delta \underline{P} = \underline{K} \, \Delta \underline{u} \qquad (19)$$

again using a simplified notation.

The residual load correction is introduced by adding the unbalanced force

$$\underline{P}^u = \underline{P} - \underline{I} \qquad (20)$$

at the beginning of an increment to the incremental equation (19) to give

$$\Delta \underline{P} + \underline{P} - \underline{I} = \underline{K} \, \Delta \underline{u} \qquad (21)$$

Clearly the residual (unbalanced) force at the beginning of the increment would be zero if the stress field used in $\underline{I}$ were in equilibrium with the external forces $\underline{P}$. This would imply that the displacement field $\underline{u}$ at the beginning of the increment is an equilibrium displacement field, provided the stresses used in (20) correspond to $\underline{u}$. This last point is now examined.

A constitutive law has been assumed to exist according to

$$\dot{\underline{\sigma}} = \underline{D} \, \dot{\underline{E}} + \dot{\underline{H}}(T) \qquad (22)$$

Adopting the Euler integration, this is written

$$\Delta \underline{\sigma} = \underline{D} \, \Delta \underline{E} + \Delta \underline{H} \qquad (23)$$

where

$$\Delta E_{k\ell} = \frac{\partial \Delta u_k}{\partial X_\ell} + \frac{\partial u_m}{\partial X_k} \frac{\partial \Delta u_m}{\partial X_\ell}$$

The stresses used in (20) are obtained from $\underline{\sigma} = \Sigma \, \Delta \underline{\sigma}$. Then these stresses $\underline{\sigma}$ are no longer the stresses corresponding to the displacement

field $\underline{u}$. For in the case of linear, isothermal elasticity,

$$\underline{\sigma} = \underline{C}\,\underline{\underline{E}} \quad , \quad \underline{C} = \text{constant}$$

with

$$E_{ij} = \frac{\partial u_i}{\partial X_j} + \frac{1}{2}\frac{\partial u_k}{\partial X_i}\frac{\partial u_k}{\partial X_j} \tag{24}$$

But the summed Euler increments give

$$\underline{\sigma} = \underline{C}\,\Sigma\,\underline{\underline{\Delta E}} \quad ,$$

with the error

$$\underline{\sigma}^e = \underline{C}(\underline{\underline{E}} - \underset{\text{incs}}{\Sigma}\,\underline{\underline{\Delta E}}) \tag{25}$$

i.e.

$$\sigma_{ij}^e = C_{ijk\ell}\Big(\underset{\text{incs}}{\Sigma}\,\frac{1}{2}\frac{\partial \Delta u_m}{\partial X_k}\frac{\partial \Delta u_m}{\partial X_\ell}\Big)$$

Thus the error is the sum of terms quadratic in the increment of displacement gradient, which for a finite element approximation are quadratic in increment of displacement. The object of introducing the load correction is to remove the quadratic error term from the incremental procedure. Since the error (25) is a sum of such terms over all previous increments, the load correction cannot be expected to improve solution accuracy unless this error is also removed. Indeed, as might be expected, the introduction of the residual load correction on the basis of stresses accumulated from the summed strain increments of (23) may lead to degradation of the solution accuracy. This was demonstrated for the one degree of freedom example of Haisler et al [29]. The results are not shown here for lack of space. Reference should be made to [16].

The difficulty is readily avoided for the elastic case by redefining the strain increment exactly:

$$\Delta E_{k\ell} = \frac{\partial \Delta u_k}{\partial X_\ell} + \frac{\partial \Delta u_m}{\partial X_k}\frac{\partial u_m}{\partial X_\ell} + \frac{1}{2}\frac{\partial \Delta u_m}{\partial X_k}\frac{\partial \Delta u_m}{\partial X_\ell} \tag{26}$$

This form of ΔE may then be used in (23) to generate the stress increments. For the elastic-plastic case the problem is not so straightforward. However the combination of (25) with the 'mean stiffness' and 'mean normal' corrections described in [32] above has been shown to be satisfactory (see, for examples, [32]). In fact the elastic-plastic problem is rather more easily controlled, because the total stress is not so directly dependent on total strain in yielded regions.

Case Studies

In this section we present a small selection of test cases to assess the accuracy of the techniques used in the program. This is then followed by the case study of two welding examples. We should keep in mind the fact that the two thermal examples considered adopted extreme impulse boundary conditions. All corresponding analytic models began with step-shaped temperature distributions which cannot be modeled accurately by a finite element mesh (which interpolates the temperature field continuously and differentiably within an element) unless a special asymptotic mesh is developed for the beginning of the solution.

Example 1: The Weiner Problem [23]

This problem is of value because it is a deliberate attempt to model a simple but realistic fusion situation for steel. Both analytic [23] and experimental results [34] are available so that the accuracy of the basic modeling assumptions (uncoupling, etc.) may be assessed. The problem is that of a half-space of molten steel at 2945°F, suddenly brought into contact with a half-space chill at 70°F, (the chill is assumed to be made of the same steel as the cast). The geometry and material properties assumed are shown in Fig. 1. Nonlinear specific heat and thermal conductivity were assumed. In [23], as in the present work, fusion was assumed to take place over a temperature range.

The predictions of the histories of solidus and liquidus positions are shown in Fig. 2. The agreement with the analytical solution is close, but the fact that general agreement with experiment is achieved is more significant. Figure 3 shows the finite element predictions of temperature profiles at different times. The severe gradient discontinuities may be seen. It is interesting to note that Weiner's solution is based on the imposition of a constant temperature at the interface. The finite element model has no such boundary condition but reproduces this assumption quite well: a constant temperature point is seen at a small distance from the original interface. This agreement is rather surprising. It is not clear whether the position of the constant temperature point in the finite element results more truly represents the real situation than Weiner's boundary condition. However, it is probable that the constant temperature point should be closer to the interface than the finite element model predicts. This is because the fixed grid model cannot reproduce exactly the initial conditions just after contact: continuity of temperature across the (finite sized) element next to the interface in the cast requires that the solution start with the fusion fronts some distance from their true position on the interface. Thus on the basis of energy balance the fixed grid finite element model introduces a geometrical shift in the solution.

This example demonstrates that in a one-dimensional case very similar to the situation under study the thermal model is able to predict experimental results to the same order of accuracy as the experimental measurements can be made. This does not necessarily imply that the model is adequate for the welding problem, because it is possible that the weld problem is more critically dependent on solution of this part of the history. Nevertheless this result gives some confidence in the technique.

Example 2:   The Two-Dimensional Square Plate Fusion Problem

This problem was chosen to illustrate a two-dimensional solution. The

problem is very like the Stefan problem in two-dimensions, except that a finite

region is studied. No exact solution exists, although some approximate solutions

are available; [20, 35, 36]. The finite element mesh and the boundary conditions

and material properties are shown in Fig. 4. An octant of the problem was

modeled to give a better idea of the performance of the method when modeling

non-simple geometries. The resulting prediction of solidus and liquidus positions

along the diagonal and normal bisector of an edge are compared in Fig. 5 with the

various other approximate solutions. The finite element results show general

agreement at later times with the results of Allen and Severn [36] and

Lazaridis [20]. The oscillations observed in the finite element results arise

because the mesh used fails to provide sufficient discontinuity surfaces to pro-

duce a smooth result on the time scale used. The properties chosen were those

used by Poots [35]. The latent heat effect is very severe (the ratio of the spe-

cific heat outside melting range to the internal heat rate within melting range

is 1/700). With respect to the typical properties of steel, the properties chosen

in this example (in particular, the latent/specific heat ratio) represent an

extreme discontinuity. Thus any element containing a fusion region is unable to

respond until the energy of that fusion region has been removed from the element.

This effectively constrains the nodal temperatures for that element, so that nodal

temperatures change rapidly as the fusion region propagates from one element to

the next, but remain essentially constant as the fusion region traverses an element.

This results in the wavy form of the solidus and liquidus time histories: clearly

these can only be accurately placed to within the order of size of the elements.

For the welding stress analysis, the significant part of the thermal

fusion problem solution is the definition of initial conditions for the lower

temperature (later time) part of the solution. Some indication of the accuracy of the present technique may be obtained from Fig. 6, where the temperature predictions at two points are given as functions of time. While the fixed grid finite element solution is inaccurate at early times, later on the agreement with previous work is reasonable. Thus it appears that the overall energy distribution is essentially maintained through the solution.

Example 3: Thermally Loaded Plate

This problem is taken from Landau et al [37] and is that of an infinite plate, 3 ft. thick, initially at a high temperature (but not above any phase transition), then cooled to room temperature by linear convection from both surfaces. The material is linear elastic-perfectly plastic, with the yield stress as the only temperature dependent property.

Initially the plate is at a uniform 1500°F. The same finite element mesh was used for both the transient thermal analysis and the stress analysis. This consisted of 20 equal sized axi-symmetric elements all with one edge on r = 0 , modeling one half of the plate thickness. The axisymmetric model was used in order to reproduce the traction boundary conditions with ease.

The thermal problem for the half plate, then, is one dimensional and linear, with an insulated boundary at x = 0 , and convection at x = 1.5 ft. The lowest order two-dimensional isoparametric element was used (linear Lagrange interpolation in the mapped plane): in one dimension this reduces to linear interpolation between nodes. A small time step of 0.05 hrs. was used to give good temperature definition for the stress analysis. The solution was run to t = 20 hrs , when all points of the mesh were below 100°F (room temperature was assumed to be 70°F): centroidal temperatures were then reduced to room temperature in an additional linear step.

The boundary conditions for the stress problem are: traction free surfaces at $x = 0$, $x = 1.5$ ft., and generalized plane strain normal to the x-direction, with no associated normal force. The latter condition was repro- duced by use of axi-symmetric elements with one set of edge nodes at $r = 0$ constrained to zero radial displacement, while the opposite edge nodes are tied together with the linear constraint condition described in reference [24]: this ensures all these nodes have the same (unspecified) radial displacement with zero integrated normal traction.

The residual stress at 70°F (assuming the material to be stress-free at 1500°F) is shown in Fig. 7. The centroidal values of stress from the finite element model agree closely with the solution of [37]. Figure 8 shows the growth of plastic zones as a function of time. The time scale is non-linear here, since it is taken to be proportional to the increment number in the stress analysis.

The only significant discrepancy between the finite element solution and that of the reference is the lack of a yield zone in the centre of the plate at late time in the finite element solution. It is clear from Fig. 7 that the inside two elements are very close to yielding at the end of the finite element solution, so that the discrepancy is rather small. It is prob- ably caused by the interfacing technique which prepares the temperature data for the mechanical analysis: this has a tendency to reduce spatial temperature gradients because it reduces a temperature-time curve to a series of secant approximations.

It is evident from this example that the finite element model is able to reproduce the analytic solution with accuracy. However, caution must be exercised in using this comparison as a guide to the accuracy of the solutions in the sample weld problems, since the latter are two-dimensional models and involve rather more complicated material behavior.

Example 4: Axisymmetric Weld

The numerical model developed was used to follow the histories of two sample welds so that comparisons could be made with experiment. Few of the experimental studies of weld residual stress and distortion contain sufficient definition of the process for the boundary conditions of the numerical model to be accurately defined. The study by Corrigan [38] does define the weld parameters fully, and in view of Tall's [2] conclusion that residual stresses depend most critically on the heat input, was chosen for the present study.

In [38] Corrigan conducted extensive experimental investigations of the residual stresses in high strength steels. The weld which was chosen as one example for the present work is a circular bead weld on an 1/2" plate of 11 5/8" diameter made from HY130-150 steel. The geometry of this configuration is shown in Fig. 9. This is one of a series of thin plates which was tested (1/2" compared to 1" for other cases), in which the assumption of plane stress was more likely to be valid. The assumption of plane stress is necessary for the analysis of the Sach boring technique.

The weld was modeled as an axi-symmetric geometry with axi-symmetric stress distribution. Corrigan has some discussion on the validity of this assumption, and justifies it experimentally. Because the welding rate (20 ins/minute on a 3" radius) is such that the conduction of heat through the steel ahead of the weld torch is negligible, each section sees essentially the same thermal history. In the model, this implies that the heat input of the torch must be applied to the model as it is assumed to be seen by any radial slice of infinitesimal tangential thickness. This is the basis for the boundary conditions discussed later.

This problem is one of the few thermal stress problems for which it is reasonable to use the same mesh for the thermal and for the stress analysis:

this mesh of the lowest order isoparametric element is shown in Fig. 10. The mesh used was rather coarse for the anticipated gradients but was thought to be a reasonable compromise with computing cost. The shape of the weld bead was taken from a macrophotograph of the section of the weld given in [38].

5.2 Material Definition

Because of the assumptions made duing the development of the numerical model, the only properties which are necessary to describing the material are: Specific heat, thermal conductivity, latent heat, solidus and liquidus temperatures, Young's Modulus, Poisson's Ratio, yield stress, workhardening modulus and secondary creep relation.

The general variation of most of these properties with temperature is discussed in some detail by Tall [2] who made a comprehensive literature survey on the topic. The properties used in the present work are assumed on the basis of [2], and from the ASTM special publications on elevated temperature properties of steels, [39], [40]. Base mechanical properties for HY130-150 were taken from [41]. It is apparent from the stress-strain curve of that publication that this steel may be considered as perfectly plastic up to 3% strain, above which the hardening is quite slow (about 50,000 psi modulus). Since strains above 2 - 3% accumulated plastic strain were not anticipated, a perfectly plastic material was assumed. In fact some elements showed accumulated plastic strains of the order of 6%, but this mostly occurred at high temperatures (above 1500°F) where the strength was very low. The range of variation for carbon steel is not extensive, so that it is probable that the properties used, as shown in Fig. 11, are within 20 - 30% of the true values. The thermal properties around the melting range are those used by Weiner [23] for .3% carbon steel (HY130-150 has .1% carbon [38]) while the

mechanical properties are extrapolated linearly from the values about 1200 -
1500°F so as to give zero strength ($E \to 0$, $c_\gamma \to 0$) at the melting range, and
a high Poisson's ratio (to approach incompressibility in the liquid phase).

Secondary creep data for HY130-150 were not found, so that a non-linear
Maxwell model was assumed, and the constants chosen to give a minimum least
square error fit to the available data at 1000°F (the stress relief temperature
used by Corrigan) for SAE-4340, for which considerable high temperature data
are available. The data and the fitted non-linear Maxwell law are shown in
Fig. 12. This creep law is not expected to be of the same order of accuracy
as the other material data.

In order to obtain an axi-symmetric model, the time variation of the
heat input from the torch was modeled as it passes over a fixed radial line in
the base metal. For this it was necessary to know the physical size of the heat
flow area. It was assumed that this was of the same order as the weld bead it-
self, so that the heat input shown in Fig. 13 was assumed. This input is con-
sistent with the total rate (20 ins/min) and the total heat input (600 BThU)
used. The heat rate was then applied to the surface and throughout the weld
bead, proportionately to the surface area of each 'layer' of nodes: this was
done in an attempt to model the 'puddling' of the weld bead. Finally the intim-
ate contact was assumed to take place at the time when the heat input rate became
zero. It might be more accurate to introduce the intimate contact layer by layer
over the 5 sec span of the heat input. In any case since the temperatures are
very high in the immediate neighborhood of the bead at this time, it is unlikely
to make a significant difference in the stress results.

The remaining thermal boundary conditions are the surface cool-
down parameters. Clearly radiation will be an important effect at such high
temperatures, so that this was introduced over all surfaces with an assumed

emissivity of .6 (taken from Sparrow and Cess [44] as typical for steel which has seen repeated heating and cooling) and a unit form factor. Convective cooling was also assumed on all surfaces. A convective-constant of 2×10^{-6} BThU/in^2 sec°F was taken for most parts of the history, except for the weld-side surface during the 60 sec of weld deposit, when a large volume of gas (50 cu. ft/hr) is blown over the surface from the weld torch. To take some account of the additional heat removal due to this flow, a constant of 1.5×10^{-5} BThU/in^{2}sec°F was used for the weld side surface during the first 60 seconds. It should be noted that these are very approximate numbers, and are simply order of magnitude assumptions. The surrounding temperature was taken as 70°F throughout, for both radiation and convection. During the mechanical analysis the disc was taken to be traction free throughout.

A simplified model was adopted for the stress relief. The disc was assumed to reach 1000°F from room temperature in a uniform manner (that is, negligible thermal gradients throughout), with no creep during this time. It was then allowed to creep as a non-linear Maxwell material for 2 hours (the time given for stress relief in the experiment), then reduced uniformly to room temperature without any further creep. Apart from the material behavior, the main assumptions are that any additional stresses caused by thermal gradients during the heat-up and cool-down times are not significant, but that the heat-up and cool-down times are sufficiently short that creep at intermediate temperatures during these times may be neglected. Although these are conflicting assumptions, they are judged sufficient in view of the uncertainty in definition of creep behavior.

The results of this particular study are interesting, because of the wide discrepancy between the experimentally obtained stress patterns and the finite element predictions. In Figs. 14 and 15 the experimental tangential and radial stresses are shown as functions of radius. The same graphs show the

range of stress on each section of element centroids in the finite element mesh.
The experimental results show an unusual pattern which Corrigan found in this
case (HY130/150) and in the case of a 12% nickel maraging steel. This 'rabbit
ears' residual stress pattern in the dominant stress (tangential) after weld-
ing had never previously been observed. Indeed the finite element results are
typical weld residual stress patterns ([2, 38, 42, 43]): the stress picture is
dominated by the stress component parallel to the weld, with this component
reaching its maximum tensile value through the fusion regions, this value being
about the room temperature tensile yield stress.

In Fig. 16 the equivalent plastic strains predicted by the finite element
model are shown as contour levels through the disc. This strain measure is
intended as a cumulative measure of damage: it is the sum of the increments of
equivalent plastic strain, $\Delta\bar{\epsilon}^P = \sqrt{\frac{2}{3}\,\Delta\epsilon_{ij}^P\,\Delta\epsilon_{ij}^P}$, so that any plasticity at a
point increases its value at that point. The picture shows that values of
5 1/2% are obtained in those elements in the base material just below the
weld bead/base interface. This value is probably rather high, and may have
been caused by the model of the heat input boundary condition (Fig. 13)
This boundary condition caused peak temperatures in the bead of the order
of 4500°F, which seems excessive, and which in turn created extremely sharp
temperature gradients around the interface. In the second example (1" HY80
plate - see below) this boundary condition was altered, as shown in Fig. 13,
and the peak temperatures dropped considerably. This indicates one of the
difficulties with the model, namely that this heat input rate is a very sensi-
tive boundary condition.

An interesting aspect of the equivalent plastic strain distribution
(Fig. 16) is the extent of the plastically yielded zone. As can be seen, there
is extensive plastic deformation throughout the entire weld section. This will

later be contrasted with the results in the 1" HY80 plate (Fig. 24). The
equivalent J_2 stress, Fig. 17, shows the same pattern: very sharp gradients
either side of the weld section, with all of that section at the room tempera-
ture yield point.

The contours of the individual stress components were found to justify
the plane stress assumption made by Corrigan. However the assumption made in
[38] that there was no bending through the thickness was not verified by the
finite element results. Similarly the assumption that there was purely elastic
readjustment during the stress horing was not likely to be true for the stress
field predicted by the finite element model because of the prediction of stresses
near yield associated with high stress gradients.

The finite element model was taken through a stress relief phase, as
described above. Once again the comparison with the experimental results,
Figs. 18 and 19, shows a wide discrepancy between the two sets of results.
In both cases, however, a drop in peak stress values of 35% is observed.
Thus conventional stress relief results have been obtained: this would be ex-
pected, although the lack of an accurate creep law prohibits close analysis
of these results.

The 'rabbit ears' distribution observed by Corrigan remains unaccounted
for. The explanation offered by Corrigan is that this distribution results
from the suppression of the phase transition in HY130-150 steel: this transi-
tion may occur at temperatures as low as 400°F. In order to investigate this
possibility, the finite element stress analysis was restarted at a point where
the temperatures in the weld neighborhood were in the range 1500-1700°F. The
solution was then completed, using the same properties defined in Fig. 11 but
with the exception of the coefficient of thermal expansion, which was given
the modified temperature dependence shown in Fig. 20. The change was intended

to reproduce the suppression of the lower temperature phase change and its associated volume change. However, this modification produced very small changes in the room temperature stress distribution: nowhere were the residual stresses (as welded) altered by more than 5%. Thus the effect observed by Corrigan cannot be explained by the suggested phenomena.

Example 5: HY80,1" Disc Weld

The 1" thick disc of HY80 steel studied by Corrigan was also analyzed. The same material properties were assumed for this example as were used for the previous one, except for the yield stress which was reduced as shown in Fig. 11. The same boundary conditions were also applied except that the heat input was assumed over 6 sec. rather than the 5 sec. used previously. This last change was intended to reduce the high temperatures observed in the previous model. A similar mesh was used for this example. A few layers of elements were added to increase the thickness of the disc.

Figure 21 gives the temperature histories of the elements close to the weld. The short duration of the transient temperatures should be noted. This picture also shows the hesitation as the material melts or fuses. The as-welded residual stresses are compared in Figs. 22 and 23 with the experimental results of Corrigan. These plots show the range of stress on the sections as predicted by the finite element model, and the stress as measured experimentally by Corrigan. It is clear from these graphs that the finite element model is predicting considerable bending on the sections close to the bead. This indicates that the no-bending assumption made by Corrigan for the experimental analysis was not valid for this thicker disc. It appears from Fig. 23 that the experimentally measured radial stress is close to the mean stress predicted by the finite element method. However, the tangential stress measurement does not correspond to a mean, but favors the higher tensile side,

which is the welded face of the specimen. A high hydrostatic tension was found at the root of the weld $(\frac{1}{3}\sigma_{kk} = 54500$ psi.). This is an effect which can only be observed in a complete stress analysis, and so it would not be easy to find experimental verification (except, perhaps, if there should be a hydrostatic dependence for crack initiation). However, it is consistent with Fig. 24 which shows the equivalent plastic strain: here the region which has undergone plastic deformation is seen to be quite localized. This may be explained from the temperature histories, Fig. 21 which show clearly the reason for this localization, since the elements toward the back face never see very high temperatures and so remain relatively rigid, while the front side elements are experiencing very high temperature gradients and so must flow plastically. In this example the highest total equivalent plastic strain was only 3.7% (c.f. 6.6% for the 1/2" weld). This is probably due to the different heat rates used for the two cases (Fig. 13), which would lend support to the point made strongly by Tall [2] that the most critical boundary condition in the problem is the heat input and heat input rate.

Discussion of Results

The approximations of uncoupling and finite-element modeling of the thermal terms in the postulated energy balance, when used with approximate data (book values) of thermal properties, gave reasonable agreement with experimentally determined solid depth in a one-dimensional casting problem. The solution also agreed with an analytic model of the same situation, derived from the diffusion equation. Thus it seems that at least for the fusion part of the problem, the uncoupling and the material model were not inaccurate assumptions.

In all cases the late time (i.e. after passage of the fusion region) solutions agreed quite well with other solutions, indicating that the general energy distribution was maintained.

On the basis of the above results and arguments, the present technique is judged acceptable for use in residual stress problems (which are the main objective of this work). For other problems in which accurate definition of fusion front positions at all times is necessary it is clear that a more refined technique would be necessary. The essential difficulty is believed to be the necessity of allowing spatial temperature gradient discontinuities normal to the fusion front surfaces. This difficulty is made acute by the use of temperature as the fundamental field variable for the finite element model, because this imposes a differentiability requirement on the temperature field chosen within each element. It is this constraint which must be eased or circumvented before more accurate results may be expected.

The examples used in the thermal development indicate that the present method is able to predict the position of the fusion front with fair accuracy. For an alloy such as steel this prediction is more accurate than for a pure phase, since the discontinuities associated with latent heat effects are less when the melting range is quite broad. In any case the fusion fronts cannot be located with more accuracy than the order of the size of the element, which means that for good prediction of fusion zone extent, a relatively fine mesh must be used around the weld itself.

In both the weld examples studied, high residual stress gradients were observed in the immediate neighborhood of the weld bead. Both models exhibited the typical bead-on-plate residual stress patterns such as the dominance of the stress component parallel to the weld, high stress gradients in the close neighborhood of the bead, and a relatively large hydrostatic tension at the root of the weld.

The creep model results in the expected reduction in peak stresses: after 2 hours at 1000°F, these stresses drop by 35-40%. Because of the short

creep times involved in stress relief (usually less than 10 hours), this model

(when properly fitted to the known creep behavior) would probably furnish good

results. The results for the 1/2" disc and the 1" disc differ very considerably.

The 1/2" disc contains residual stresses which are essentially uniform across

the thickness but the stresses in the 1" disc vary drastically through the

thickness in the neighborhood of the bead. This is explained by the rigidity

of the back face of the 1" disc: because of the bead size and heat input

rate, this face never experiences very high temperatures (see Fig. 21) and so

forces the distortion to be localized around the bead (Fig. 24). It would

appear from this observation that the assumptions made for experimental analysis

by Corrigan are reasonable for the 1/2" plates, but are not acceptable for the

1" plates. The maximum cumulative damage, as measured by the total equivalent

plastic strain, is very different in the two cases, the 1/2" disc having at the

weld root 6.6% strain and the 1" disc having 3.7% at the same point. That is

explained by the different heat input boundary conditions (Fig. 13) assumed in

the two cases.

We have used a time independent plasticity theory even though this is

not the dominant mechanism high temperatures. But it has been argued that the

important stresses and distortions only arise at the lower temperatures when

the material can offer resistance to the thermally induced strains. Moreover,

at intermediate temperatures (say from 800-1200°F for steel) the time-independ-

ent theory is based on materials data (yield stress) which is obtained through

tests controlled over the same order of time scale as is involved in the weld-

ing process, and so contains some part of the primary creep effects. It is there-

fore thought that the theory is a reasonable first approximation. It does not

account for important effects such as the temperature rate sensitivity of the

low temperature yield stress in multiphase alloys nor does it combine the

plasticity and creep effects.

To some extent the present results suggest that the theory currently used in the model is satisfactory in this first order sense. For both welds modeled, the residual stress predictions follow the patterns generally observed. However, one of the examples (1/2" disc, HY130/150) was deliberately chosen because the experimental results showed a very unusual residual stress distribution, for which the mechanism of suppressed phase change had been offered as an explanation. The numerical model was not able to reproduce this peculiar distribution when an attempt was made to include the suppression of the phase change. This is taken to indicate that phase change suppression is not the physical mechanism involved, and that this mechanism is not contained in the numerical model. It is interesting to speculate that those unusual patterns observed in the experiments were the result of micro-cracking, since this steel (HY130/150) is prone to such failure. As yet no crack criterion has been included in the model. Thus the difficulty with this result has not been resolved.

So far this work has not discussed the problem of weld dressing. The welds examined above were not, in fact, dressed in the experiments, but the dressing process is usually a part of welding in structural fabrication. It is not yet clear whether this process has an important influence on the residual distortion and stress patterns, although it may be anticipated from the very high stress gradients close to the surface that dressing will alter the stress distributions significantly. In fact it should not be difficult to introduce a simple model of this process. One possibility is to compute the reactions at the nodes of an element in the 'dressed off' part of the mesh, as is done for the residual load correction, then to remove that element, replacing it with the reaction forces which are then reduced to zero over some increments.

It is clear that the present results are in agreement with Tall's conclusion [2] that the residual stresses are most sensitive to the primary heat input boundary condition. In more recent work a better definition of this boundary condition has been achieved by comparing finite element predictions of fusion zone extent with post-weld macro-photographs, in which the extent of the fusion zone may usually be readily seen. Then such parameters as are efficiency and are size are adjusted to give reasonable agreement. This technique gives some confidence in the definition of this critical boundary condition.

In view of the above mentioned extensions to the present work, it seems that the effort involved in developing the model within the context of the work on a general purpose program should prove of great value, in that these anticipated developments should all be readily incorporated into the general model.

Conclusions

It has been shown that the uncoupled thermo-mechanical finite element model of the weld process developed in this work has the ability to model several important aspects of that process. The procedure treats the thermal and mechanical parts of the process as separable, and in each part techniques have been developed to treat what are regarded as the dominant first-order effects.

a) The Thermal Analysis:

1. It has been demonstrated that the finite element model is able to predict the temperature field in solids undergoing fusion transformation to reasonable accuracy. However, the accuracy is limited by the temperature gradient discontinuities across a fusion front. The technique used essentially limits the definition of fusion front position to the order of element size for a very narrow melting range (as for a pure solid), although higher accuracy has been shown for steel, which has a relatively broad melting range.

2. The intimate contact boundary condition has been assumed for the deposition of the bead. This boundary condition allows the model to assume that the bead and base do not have the same temperature when the bead is deposited, and so is applicable to various other physical situations. This model has been shown to give reasonable correlation with experiment and analysis in the case of a one-dimensional steel solidification problem.

3. The shape change when the bead melts has not been modeled, but in the examples considered the bead has a rather uniform temperature field before it is merged into the base, so that this should not be an important effect.

4. It has been shown that a minor change in the heat input rate from the weld torch has a significant effect on the peak temperatures, because of the extremely high radiation cooling rate at the temperature of the process. Thus the results of the analysis appear most sensitive to the heat input rate.

b) The Mechanical Analysis:

1. The constitutive assumption is of primary importance in this part of the analysis. In this work it has been demonstrated that the generally observed residual stress patterns are predicted when classical time-independent plasticity theory with temperature dependent properties is assumed.

2. A simple creep formulation has been used to model the stress relief process. This has been shown to give the expected drop in peak stress values as a result of high-temperature stress relief.

3. Predicted residual stress patterns even in simple cases are quite complex. For the 1" disc agreement with peak stress values is evident, but the experimental assumptions of no bending cannot be accepted on the basis of the finite element predictions of stress. In particular the variation of the stress through the thickness in this case (where the weld depth is about 20% of the thickness) is very strong.

For the 1/2" disc the experimental assumptions are generally upheld, but there is no agreement with experimental results. The suggested mechanism of phase change suppression does not appear to cause the observed stress patterns, so that it must be concluded that these are caused by phenomena which have not been built into the numerical model.

Acknowledgments

References

1. Masubuchi, K., "Control of Distortion and Shrinkage in Welding," Welding Research Council Bulletin No. 149, April 1970.

2. Tall, L., "Residual Stresses in Welded Plates - A Theoretical Study," Welding Journal 43 (1), 1964.

3. Masubuchi, K., Simmons, F. B. and Monroe, R. E., "Analysis of Thermal Stresses and Metal Movement During Welding," RSIC-820, Redstone Scientific Information Center, Redstone Arsenal, Alabama, July 1969.

4. Marcal, P. V., "Finite Element Analysis of Combined Problems of Nonlinear Material and Geometric Behavior," Proceedings of the ASME Computer Conference on Computational Approaches in Applied Mechanics, June 1969, p. 133.

5. Stricklin, J. A., Martinez, J. E., Tillerson, J. R., Hong, J. H. and Haisler, W. E., "Non-linear Dynamic Analysis of Shells of Revolution by Matrix Displacement Method," Texas A & M University, Texas Engineering Experimental Station, Report 69-77.

6. Murray, D. W. and Wilson, E. L., "Finite Element Post-Buckling Analysis of Thin Elastic Plates," Proceedings of the Second Conference on Matrix Methods in Structural Mechanics, AFFDL, Octor 1967.

7. Hibbitt, H. D., Levy, N, and Marcal, P. V., "On General Purpose Finite Element Computer Programs," paper presented at the Winter Annual Meeting 1970, ASME, Pressure Vessel and Piping Division.

8. Greenbaum, G. A. and Rubinstein, M. F., "Creep Analysis of Axisymmetric Bodies Using Finite Element," Nuclear Engineering Design, 7, 1967.

9. Hartung, R. D., "An Assessment of Current Capability for Computer Analysis of Shell Structures," AFFDL-TR-67-194, February 1970.

10. Oden, J. T and Knoss, D. A., "Analysis of General Coupled Thermoelastic Problems by the Finite Element Method," Proceedings of the Second Conference on Matrix Methods in Structural Mechanics, AFFDL, October 1968.

11. Naghdi, P. M., "Stress-Strain Relations in Plasticity and Thermoplasticity," Plasticity, Proceedings of the Second Symposium on Naval Structural Mechanics, Lee and Symonds, eds., Pergamon Press, 1960.

12. Hoff, N. J., ed., "Creep in Structures," Springer-Verlag, Berlin, 1962.

13. Green, A. E. and Naghdi, P. M., "A General Theory of an Elastic-Plastic Continuum," Arch. Rat. Mech. Anal. 18.

14. Wilson, E. L and Nickell, R. E., "Application of the Finite Element Method to Heat Conduction Analysis," Nuclear Eng. and Design, 4, 1966, pp. 276-286.

References (cont'd)

15. Visser, W., "The Finite Element Method in Deformation and Heat Conduction Problems," Ph.D. Thesis, Delft 1968.

16. Hibbitt, H. D., "A Numerical Thermo-Mechanical Model for the Welding and Subsequent Loading of a Fabricated Structure," PhD. Thesis, Brown University, 1972.

17. Richtmyer and Morton, "Difference Methods for Initial Value Problems."

18. Carslaw, H. S. and Jaeger, J. C., "Conduction of Heat in Solids," Oxford, 1959.

19. Murray, W. D. and Landis, F., "Numerical and Machine Solutions of Transient Heat-Conduction Problems Involving Melting and Freezing, Part I, Method of Analysis and Sample Solution," Trans. ASME, J. Heat Transfer, May 1959.

20. Lazaridis, A., "A Numerical Solution of the Multidimensional Solidification (or Melting) Problem," Int. J. Heat Mass Transfer, 13, 1970.

21. Sikorskic, D. L and Boley, B. A., "The Solution of a Class of Two-Dimensional Melting and Solidification Problems," Int. J. Solids and Structures, 1, 1965.

22. Boley, B. A., "Temperature and Deformation in Rods and Plates Melting Under Internal Heat Generation," Cornell University, Report No. 4, ONR Tech. NR064-401.

23. Weiner, J. H., "Transient Heat Conduction in Multiphase Media," British J. Applied Physics, 6, 1955.

24. Hibbitt, H. D. and Marcal, P. V., "Hybrid Finite Element Analysis with Particular Reference to Axi-Symmetric Structures," Proc. AIAA 8th Aerospace Sciences Meeting, 1970.

25. Hibbitt, H. D., Marcal, P. V. and Rice, J. R., "A Finite Element Formulation for Problems of Large Strain and Large Displacement," International Journal of Solids and Structures, August 1970.

26. Zienkiewicz, O. C., Valliapan, S. and King, I. P., "Elastic-Plastic Solutions of Engineering Problems 'Initial Stress' Finite Element Approach," Int. J. Num. Meth. in Eng., 1, 1969.

27. Marcal, P. V. and King, I. P., "Elastic-Plastic Analysis of Two-Dimensional Stress Systems by the Finite Element Method," Int. J. Mech. Sci., 9, 1967.

28. Mendelson, A., Hirschberg, M. H. and Manson, S. S., "A General Approach to the Practical Solution of Creep Problems," Trans. ASME, 81D, 1959.

References (cont'd)

29. Haisler, W. E., Stricklin, J. A. and Stebbins, F. J., "Development and Evaluation of Solution Procedures for Geometrically Non-Linear Structural Analysis by the Direct Stiffness Method," AIAA/ASME 12th Structures, Structural Dynamics and Materials Conference, 1971.

30. Hofmeister, L. D., Greenbaum, G. A. and Evensen, D. A., "Large Strain, Elasto-Plastic Finite Element Analysis," AIAA/ASME 11th Structures, Structural Dynamics and Material Conference, Denver, Colorado, April, 1970, pp. 250-259.

31. Stricklin, J. A., Haisler, W. E., Riesemann, W. A., "Formulation, Computation and Solution Procedures for Material and/or Geometric Nonlinear Structural Analysis by the Finite Element Method," Texas A & M University Report to Sandia Corporation, SC-CR-72-3102, January, 1972.

32. Rice, J. R. and Tracey, D. M., "Computational Fracture Mechanics," ONR Int. Symp. on Numerical and Computer Methods in Structural Mech., Urbana, Ill., 1971.

33. McNamara, S. F., "Incremental Stiffness Method for Finite Element Analysis of the Nonlinear Dynamic Problem," Ph.D. Thesis, Brown University, 1971.

34. Clarke, K. L., Trans. Amer. Foundrymen's Assoc. 53, 1945.

35. Poots, G., "An Approximate Treatment of a Heat Conduction Problem Involving a Two-Dimensional Solidification Front," Int. J. Heat and Mass Transfer, 5, 1962.

36. Allen, D. N. de G. and Severn, R. T., "The Application of Relaxation Methods to the Solution of Non-Elliptic Partial Differential Equations," Quart. J. Mech. and Applied Math, 15, 1962.

37. Landau, H. G., Weiner, J. H. and Zwicky, E. E., "Thermal Stress in a Visco-elastic-plastic Plate with Temperature Dependent Yield Stress," Journal Appl. Mech., Vol. 27, 1960.

38. Corrigan, D. A., "Thermomechanical Effects in Fusion Welding of High Strength Steels," Ph.D. Thesis, MIT, 1966.

39. Eldridge, E. A. and Deem, H. W., "Report on the Physical Properties of Metals and Alloys from Cryogenic to Elevated Temperatures," ASTM Special Technical Publication 296, 1961.

40. Simmons, W. F. and Cross, H. C., "Report on the Elevated-Temperature Properties of Wrought Medium-Carbon Alloy Steels," ASTM Special Publication 199, 1957.

41. Willner, A. R. and Soline, M. L., "Materials Survey for the Rescue and Search Vehicles of the Deep-Submergence Systems Project," David Taylor Model Basin Report 1987, U.S. Navy.

References (cont'd)

42. Masubuchi, K. and Martin, D. C., "Investigation of Residual Stresses by Use of Hydrogen Cracking - Part II," Welding Journal, September, 1966.

43. Welding Handbook, Section 1.

44. Sparrow, E. M. and Cess, R. D., "Radiation Heat Transfer."

CHILL
INITIALLY 70°F

CAST
INITIALLY 2845°F

-2   -1   0   1   2   SCALE(ins)

GEOMETRY AND INITIAL CONDITIONS

FINITE ELEMENT MESH (LINEAR INTERPOLATION)
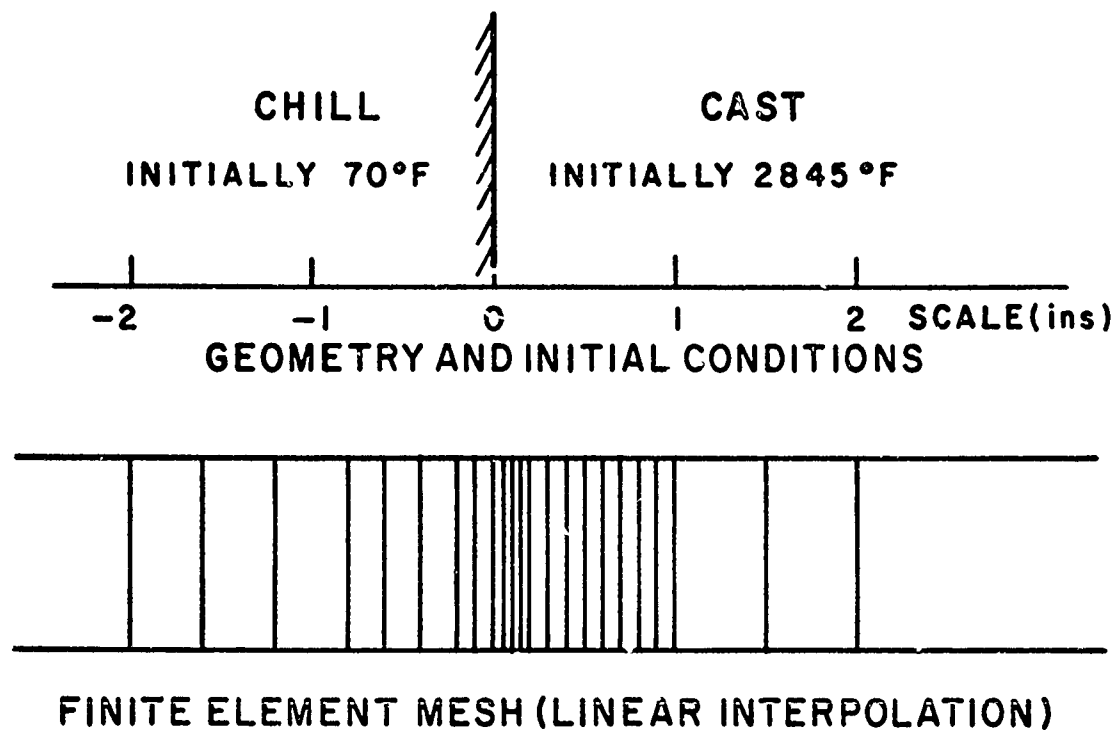
LATENT HEAT 33.56 BThU/in^3, SOLIDUS 2600°F, LIQUIDUS 2700°F

SPECIFIC HEAT (BThU/in^3 °F)

s ℓ

6×10^{-2}

5.21×10^{-2}

4×10^{-2}

4.47×10^{-2}

2×10^{-2}

0

0   1000 2000 3000
TEMPERATURE (°F)

THERMAL CONDUCTIVITY (BThU/in sec °F)

s ℓ

6×10^{-4}

4×10^{-4}

4.26×10^{-4}

2×10^{-4}

2.13×10^{-4}

0

0   1000 2000 3000
TEMPERATURE (°F)

ASSUMED MATERIAL PROPERTIES
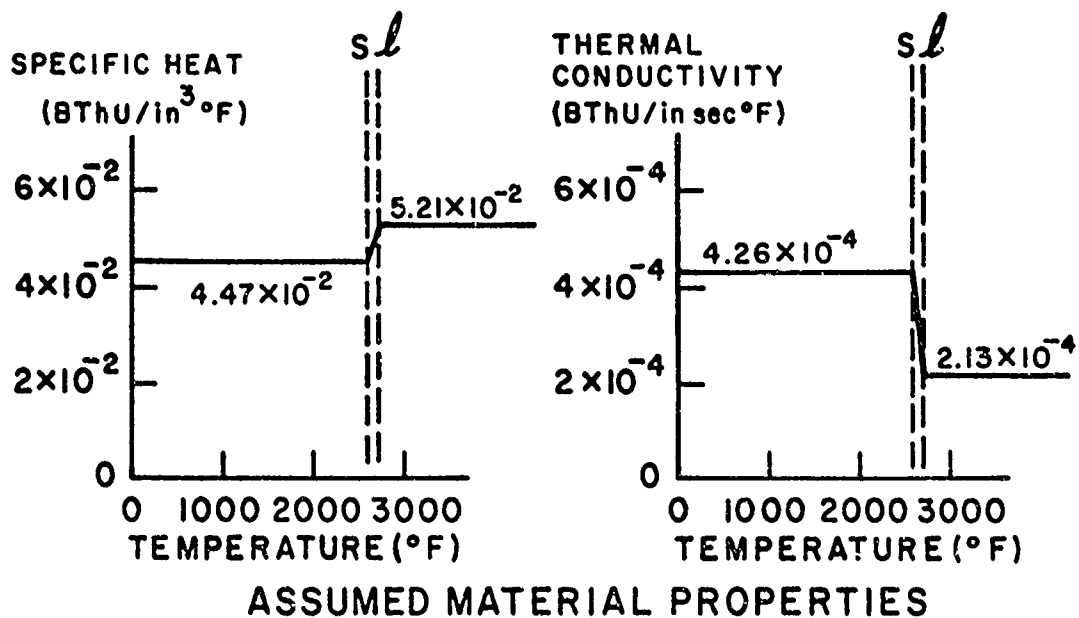
FIG. I WEINER PROBLEM (ONE-DIMENSIONAL STEEL SOLIDIFICATION)
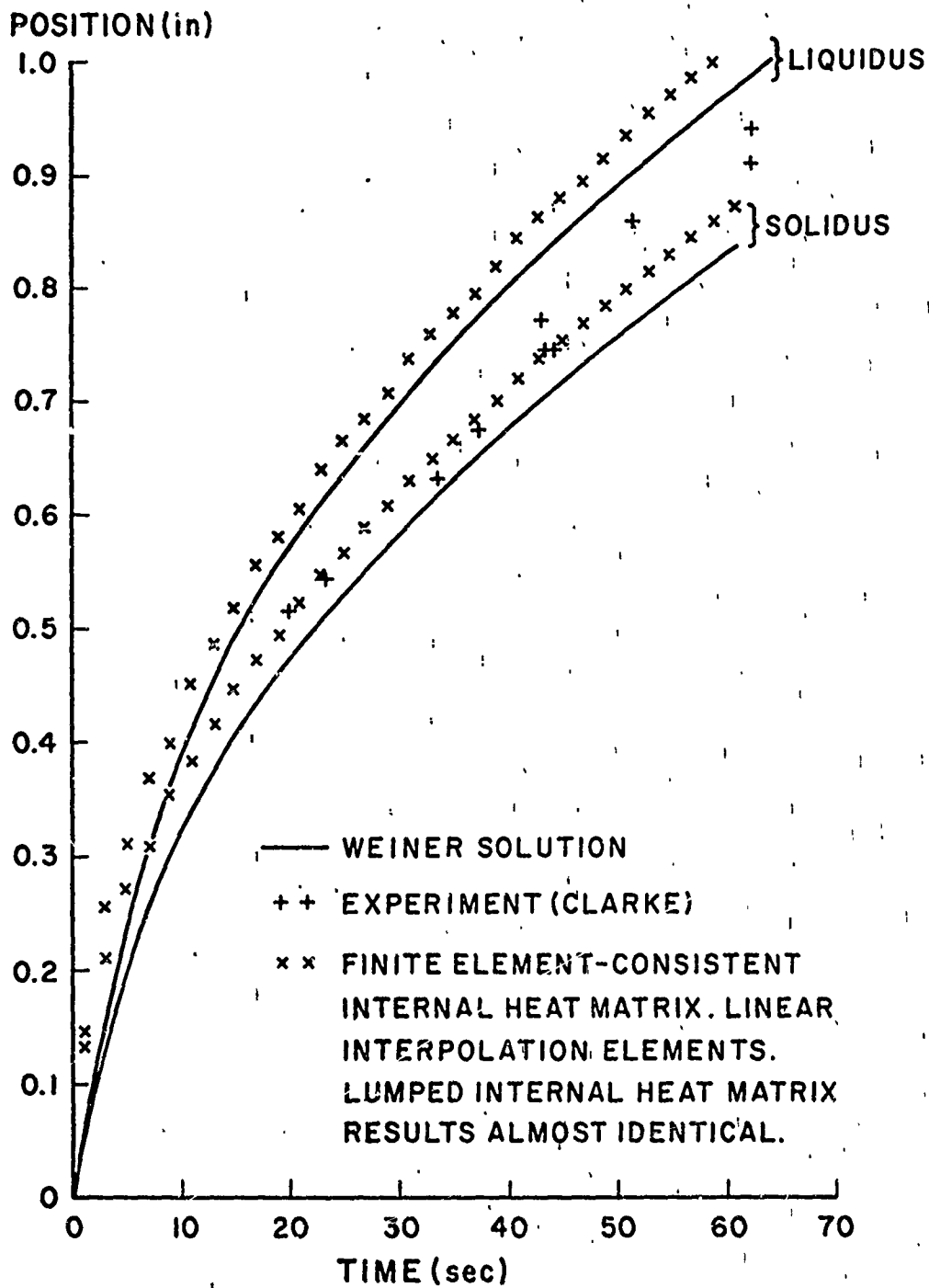
FIG. 2 ONE DIMENSIONAL STEEL SOLIDIFICATION PROBLEM
(WEINER PROBLEM)
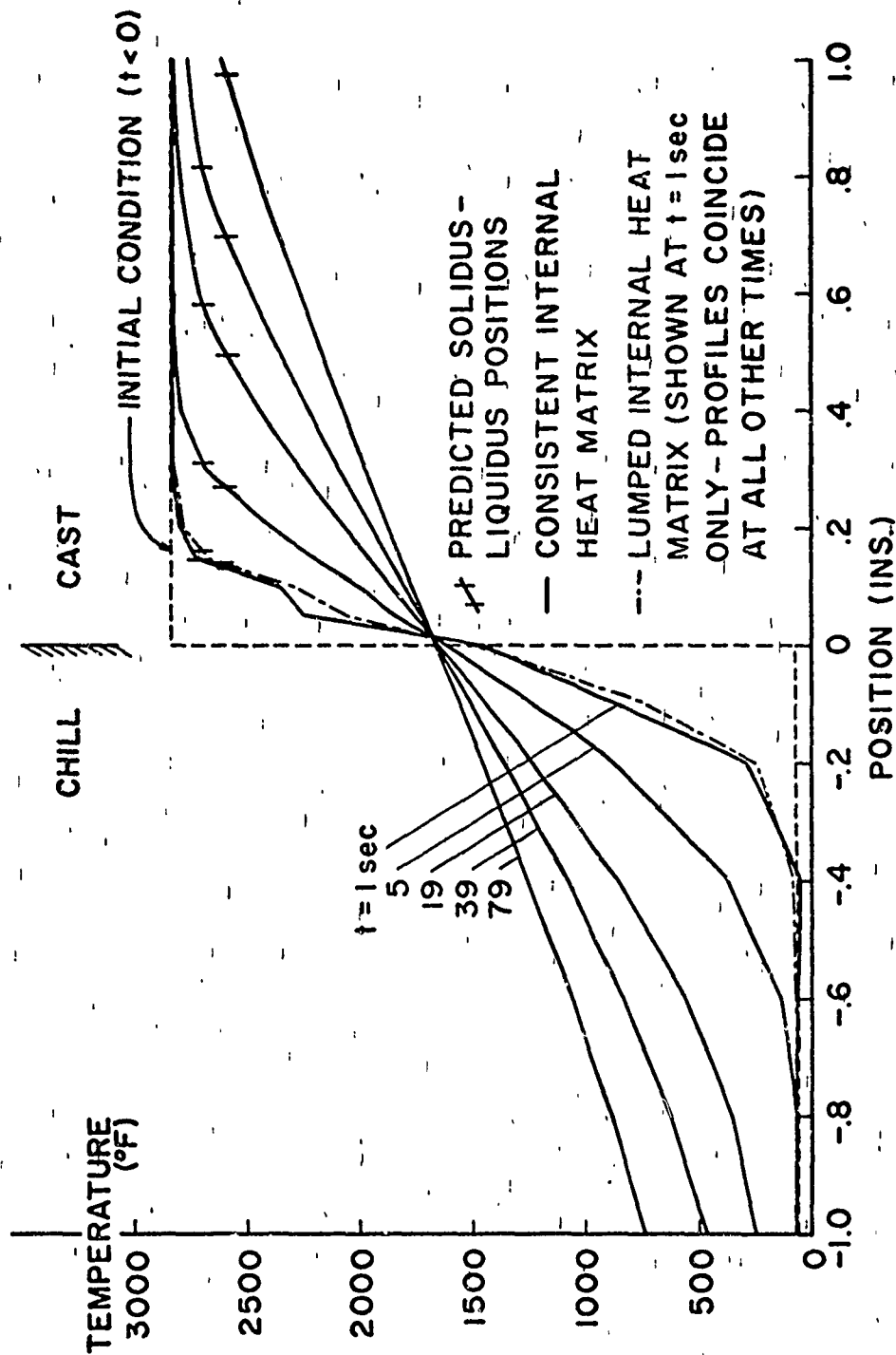
FIG. 3   WEINER PROBLEM. FINITE ELEMENT PREDICTIONS OF TEMPERATURE PROFILES.
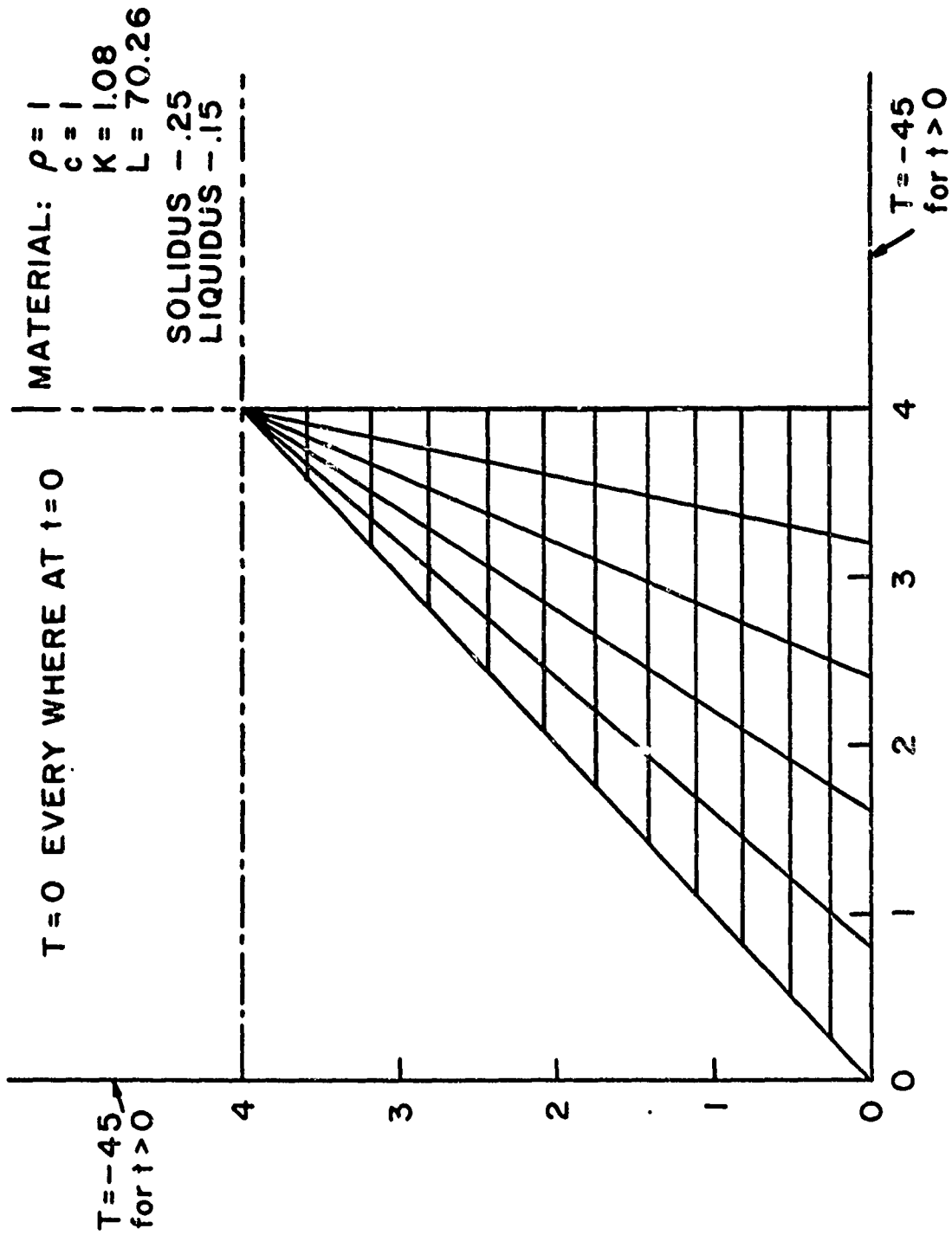
FIG. 4 FINITE ELEMENT MESH FOR 2-D FUSION PROBLEM.
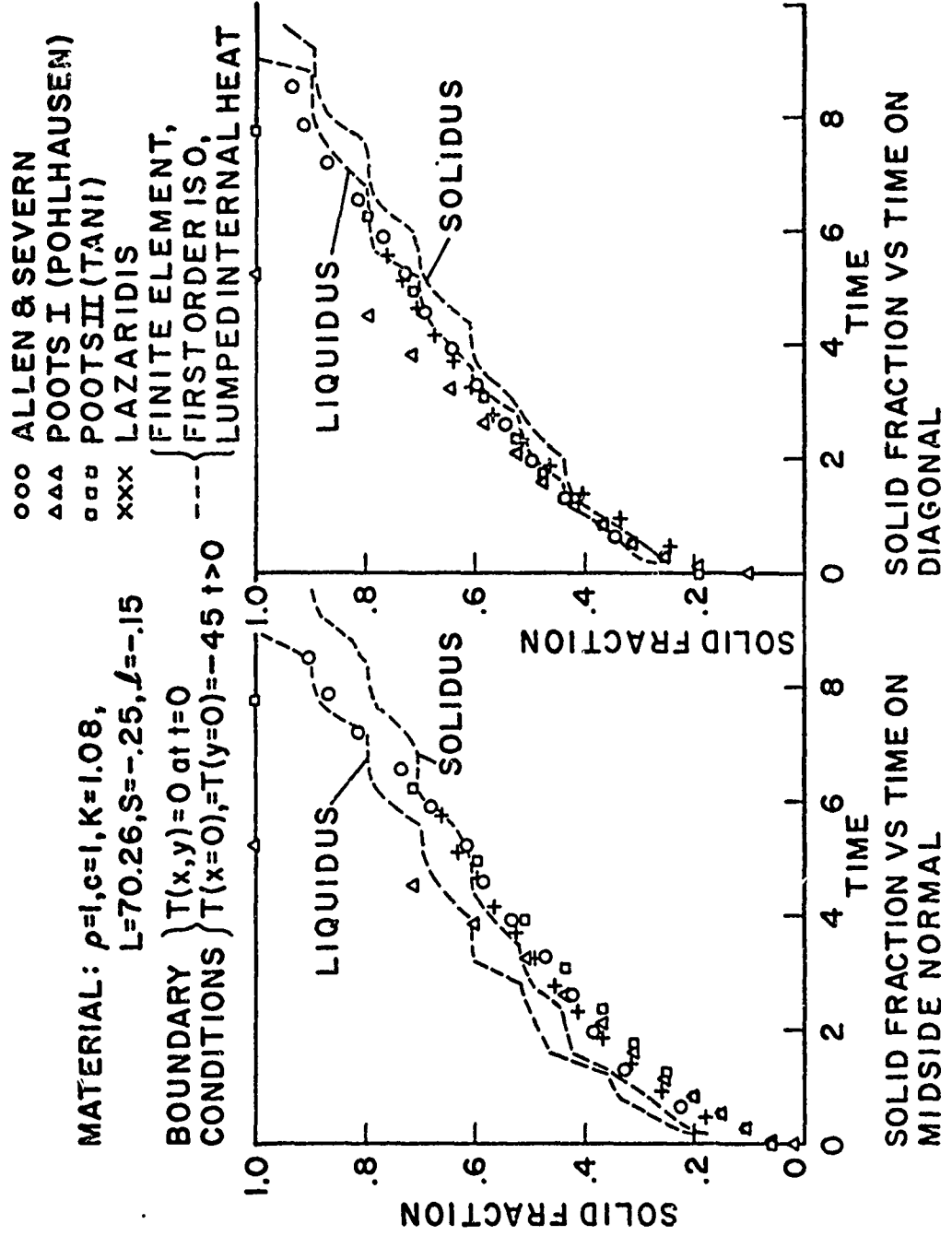
FIG. 5 TWO DIMENSIONAL FUSION PROBLEM
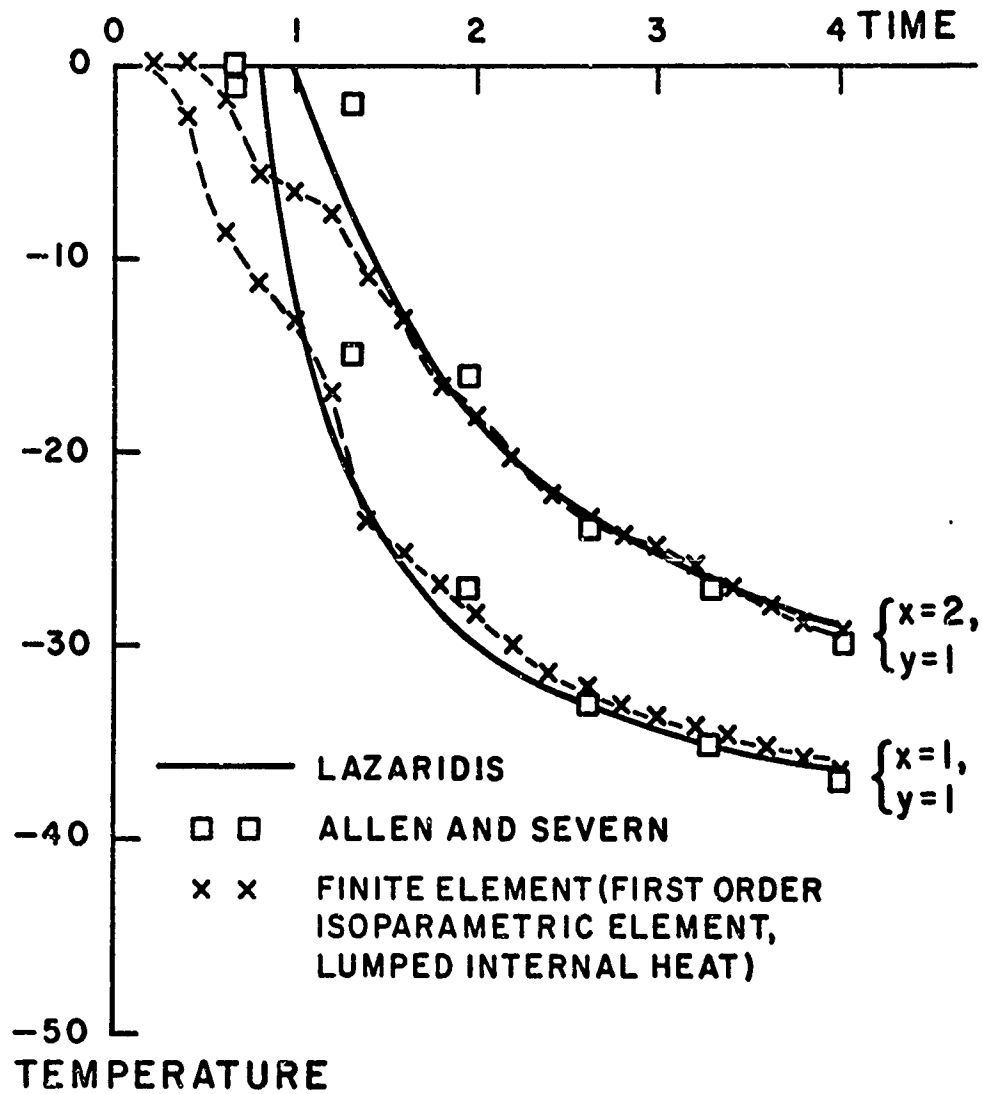
FIG. 6 TEMPERATURE-TIME PREDICTIONS
IN 2-D SOLIDIFICATION PROBLEM
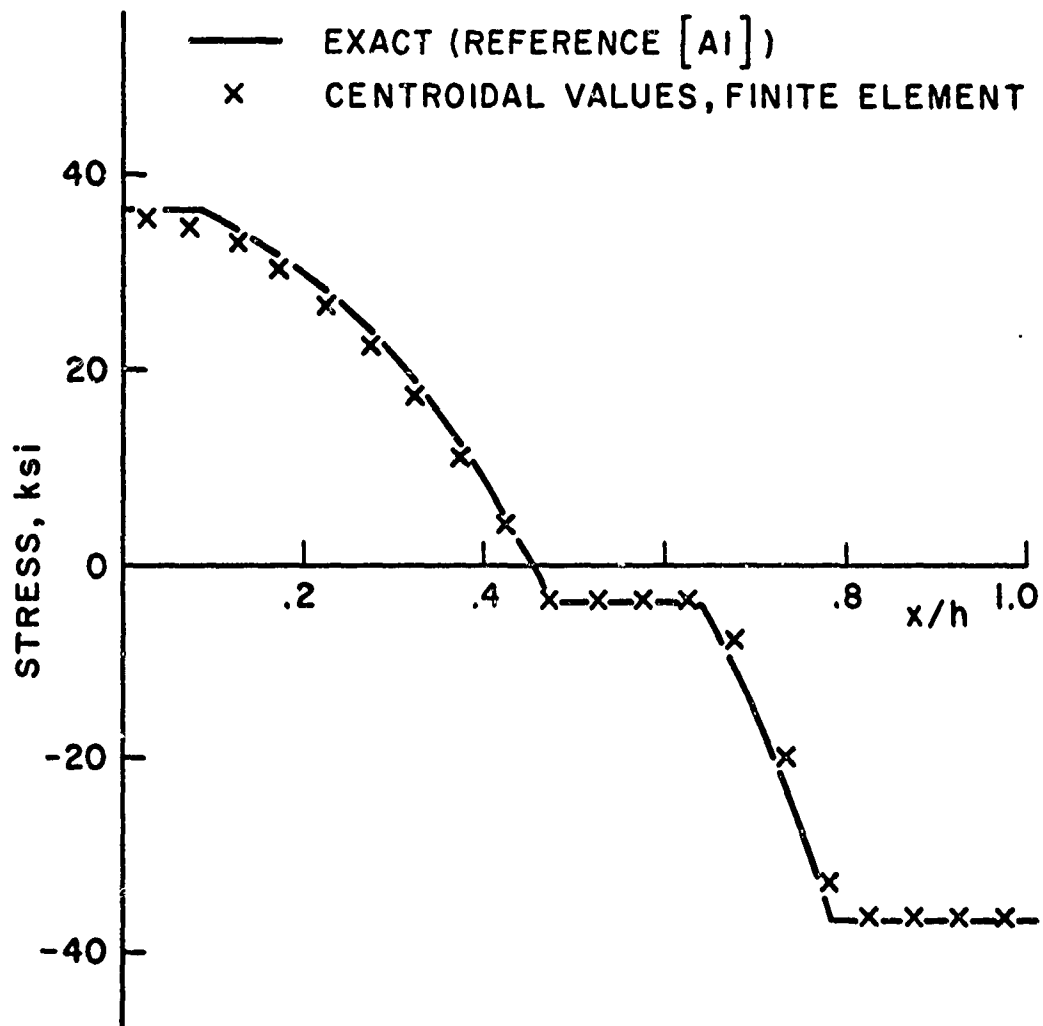
FIG. 7   RESIDUAL STRESS IN COOLED PLATE.
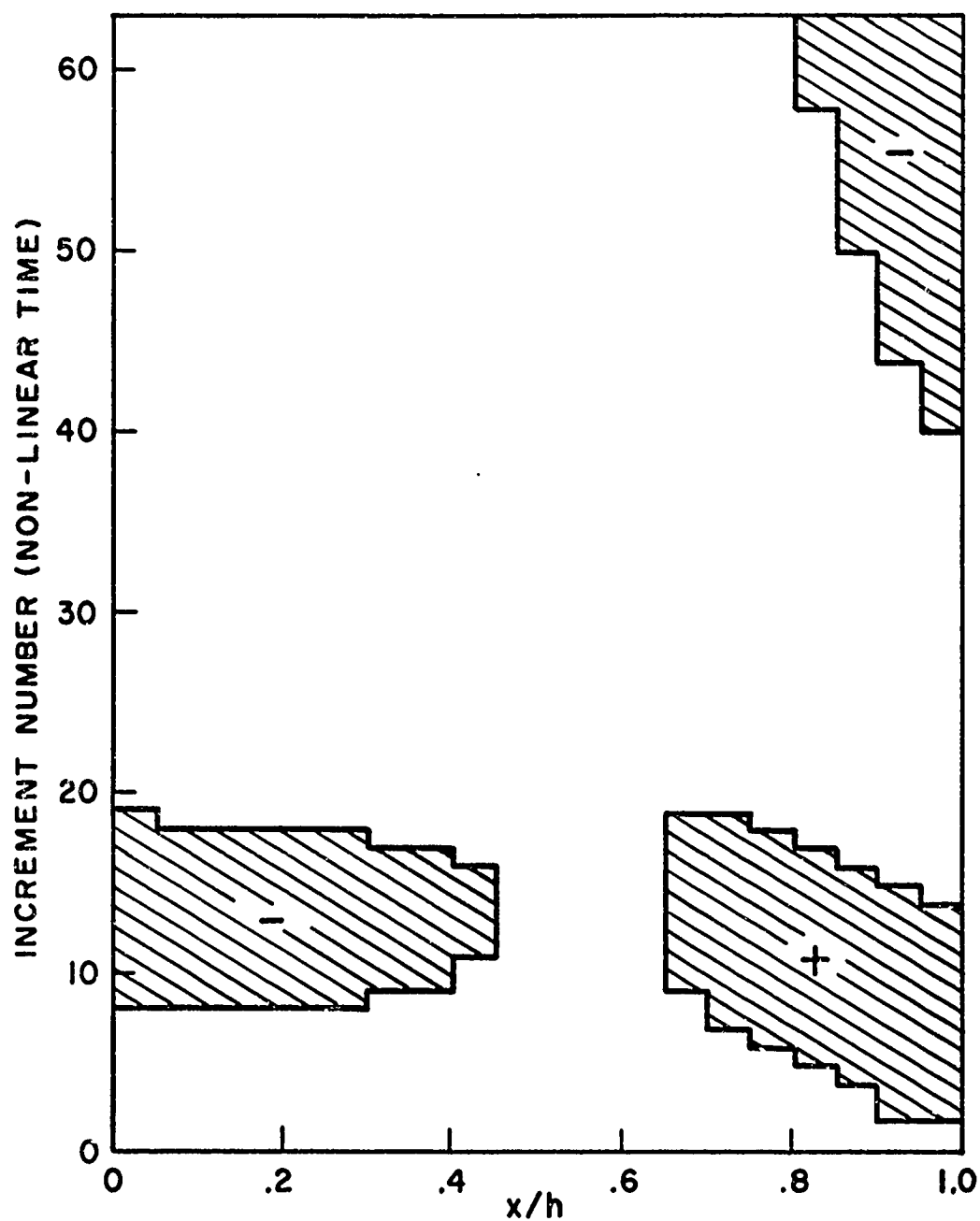
FIG. 8   COOLED PLATE: DEVELOPMENT OF
         YIELDING ZONES. (SIGN OF STRESS
         INDICATED BY + AND −).
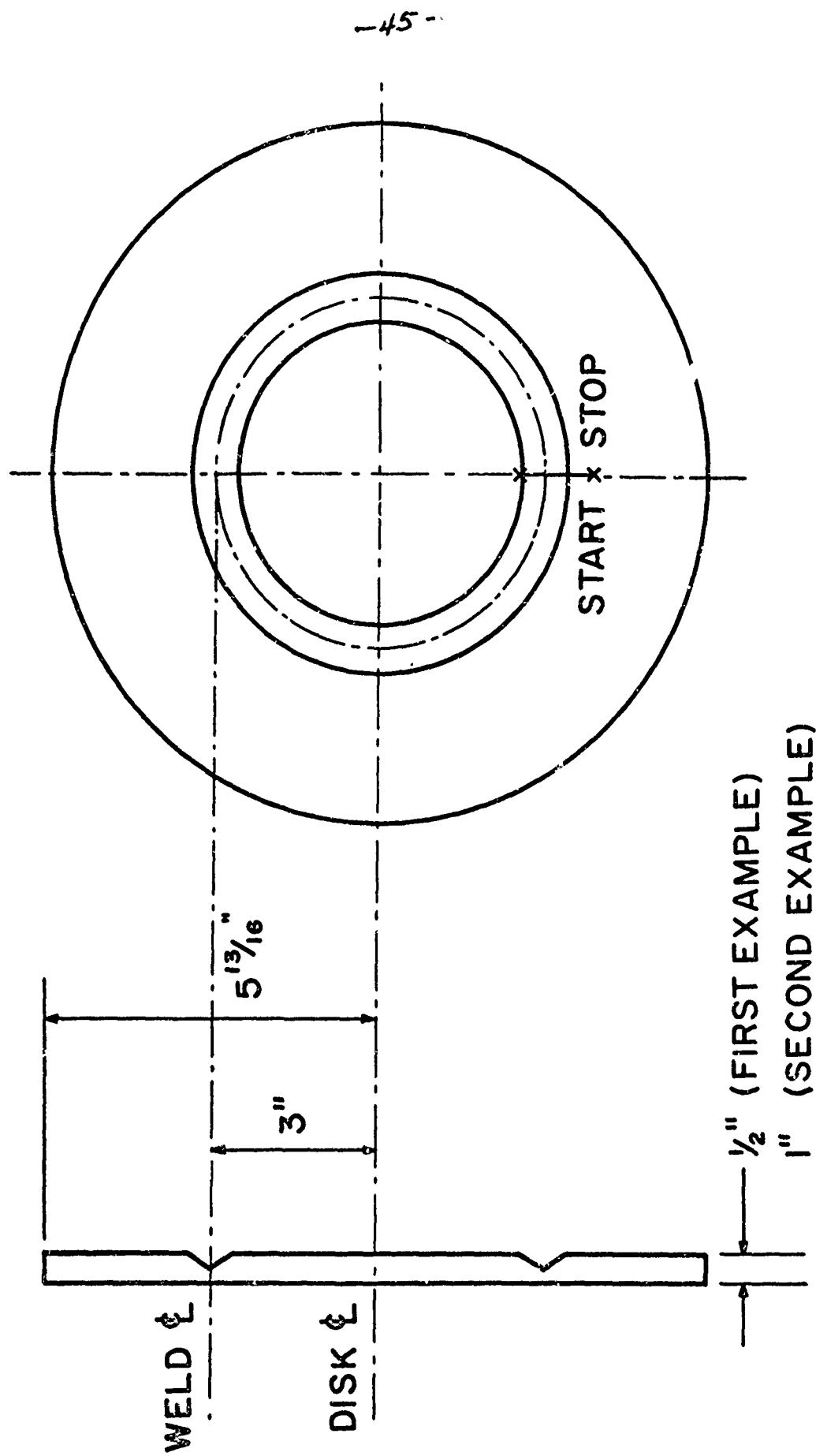
FIG. 9   GEOMETRY OF WELD.
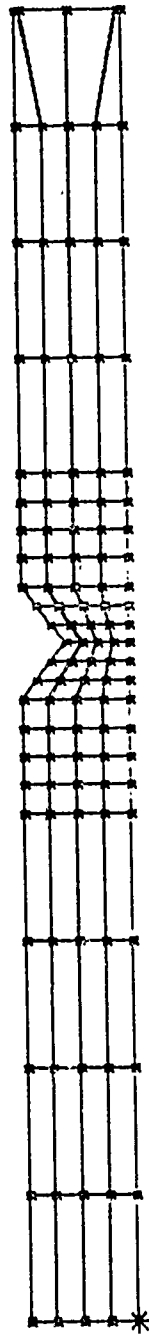
FIG. 10 WELD MESH, 1/2 INCH
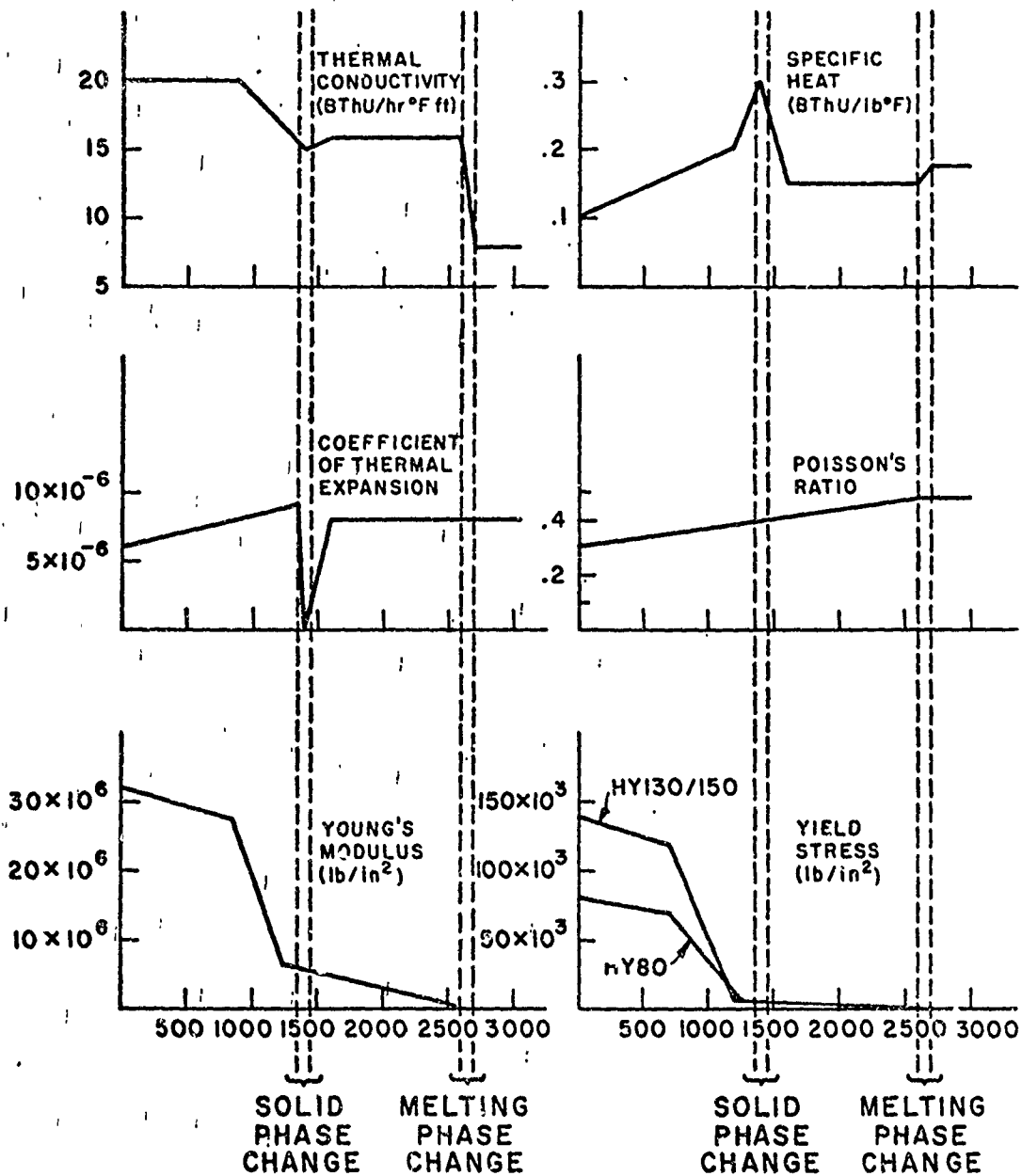
DENSITY .283 lb/in³   FUSION LATENT HEAT 118.6 BThU/lb

FIG. II ASSUMED MATERIAL PROPERTIES, HY130/150, HY80

FIG. 12 CREEP DATA

SAE 4340
x - 1000°F DATA
SHOWS FIT OF $\dot{\epsilon} = A\sigma^n$
FOR LEAST SQUARE
ERROR

$Ln(\dot{\epsilon}) = 1.883\, Ln(\sigma) - 29.31$
$\dot{\epsilon} = 1.866 \times 10^{-13} \sigma^{1.883}$

Ln (STRESS) (psi)

Ln (STRAIN RATE) (PER HOUR)
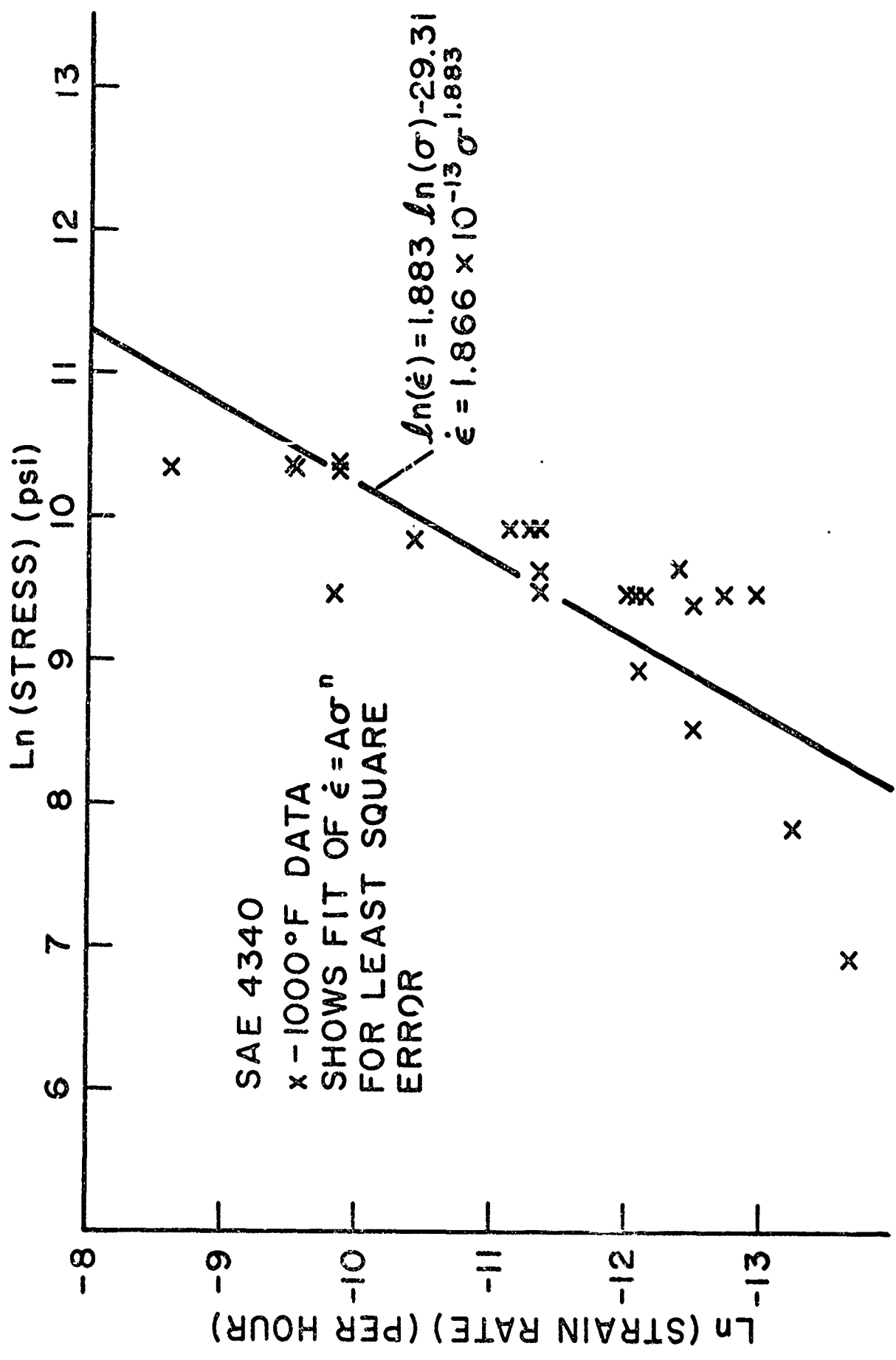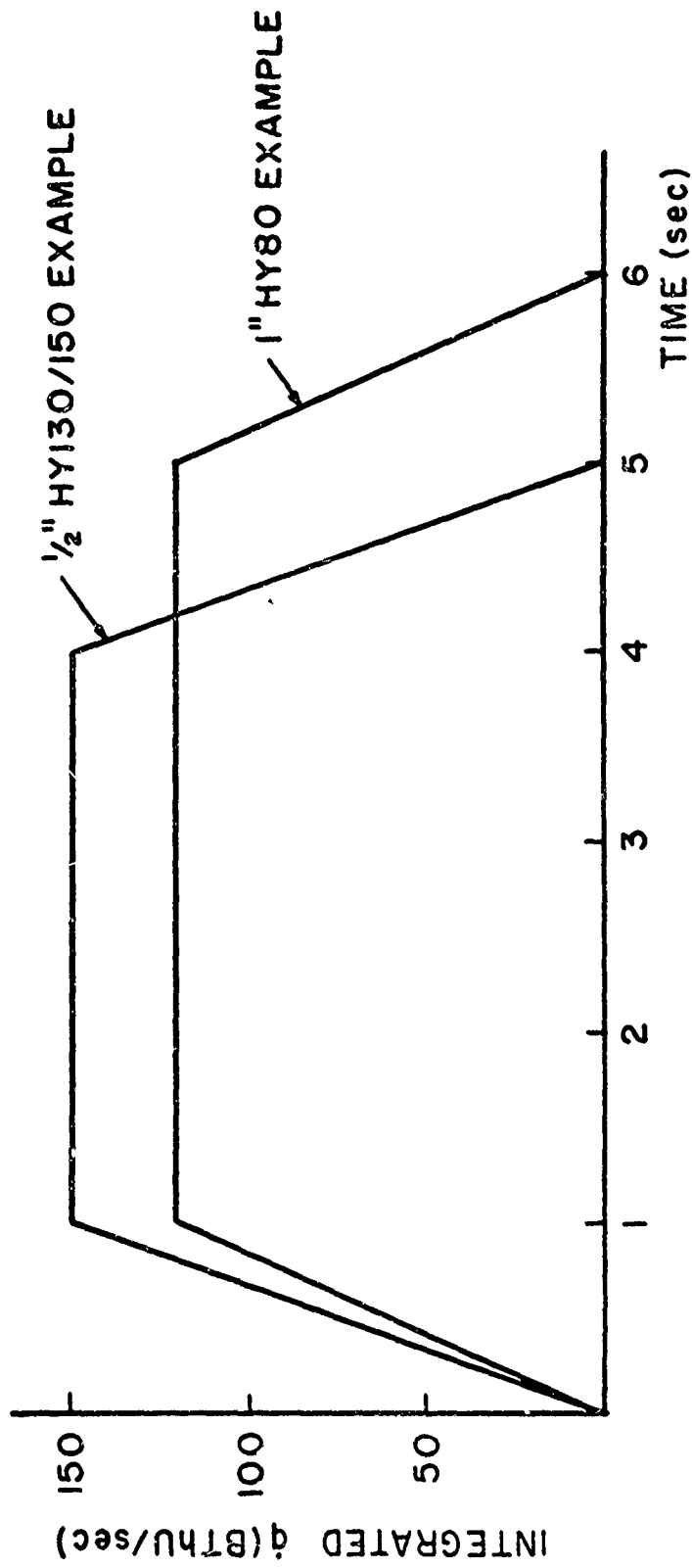
FIG. 13   ASSUMED HEAT INPUT.
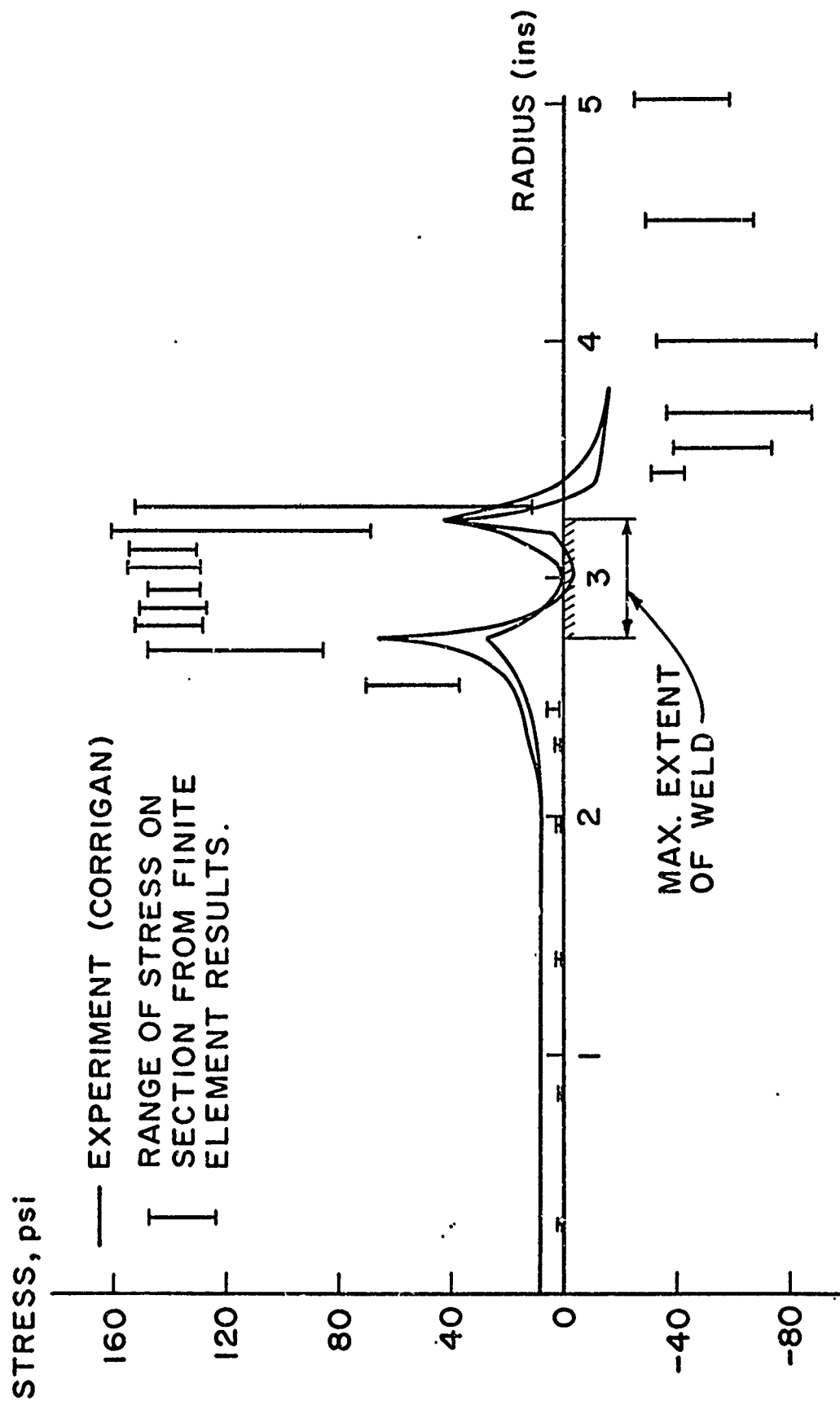
FIG. 14   AS WELDED TANGENTIAL STRESS, HY130/150, $\frac{1}{2}$" DISC.
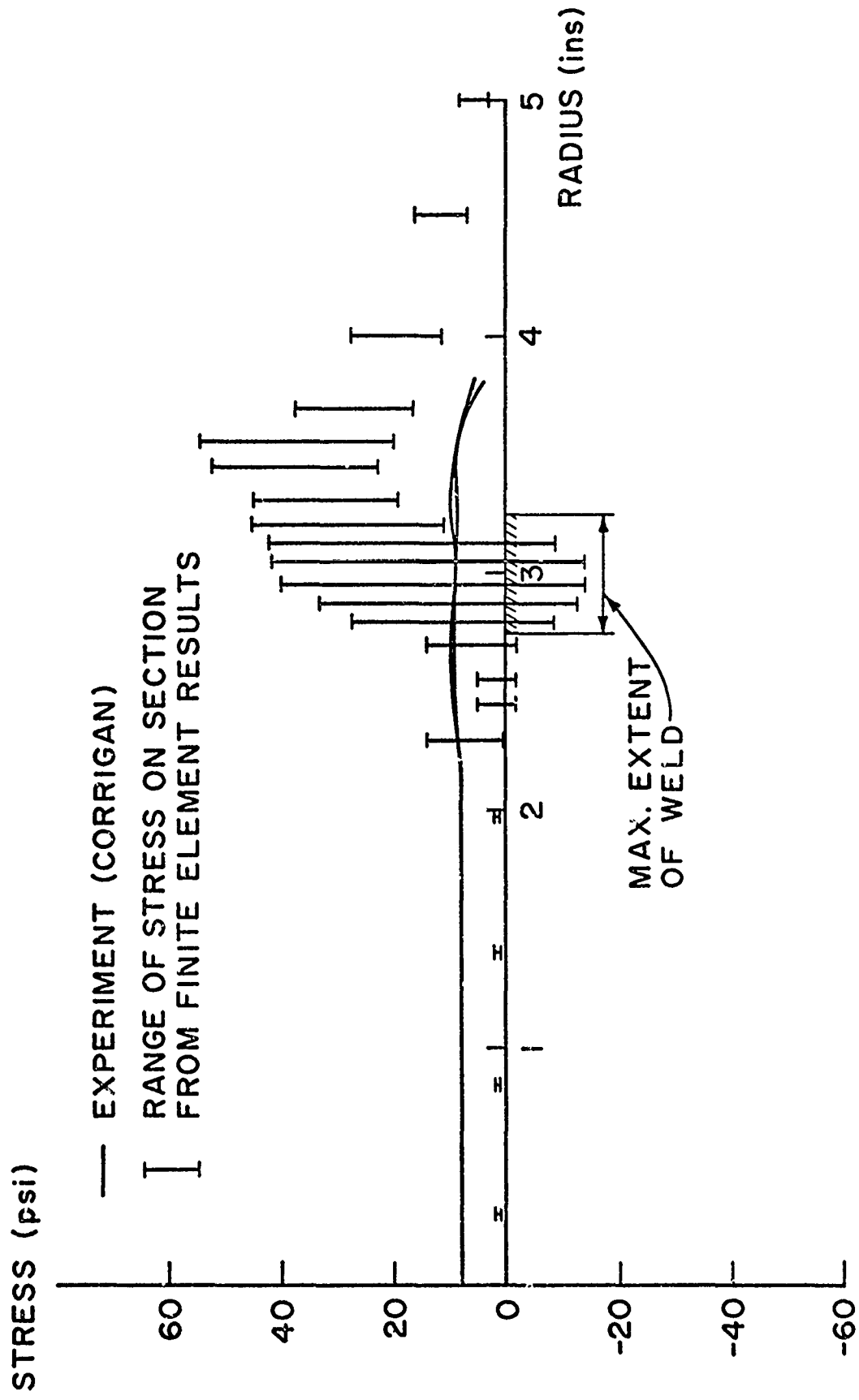
FIG. 15 AS WELDED RADIAL STRESS, HY130/150, $\frac{1}{2}$" DISC.

1/2IN.DISC AS WELDED

EQUIV PLASTIC STRAI

C(1)=0.00466
C(2)=0.01397
C(3)=0.02328
C(4)=0.03259
C(5)=0.04190
C(6)=0.05121
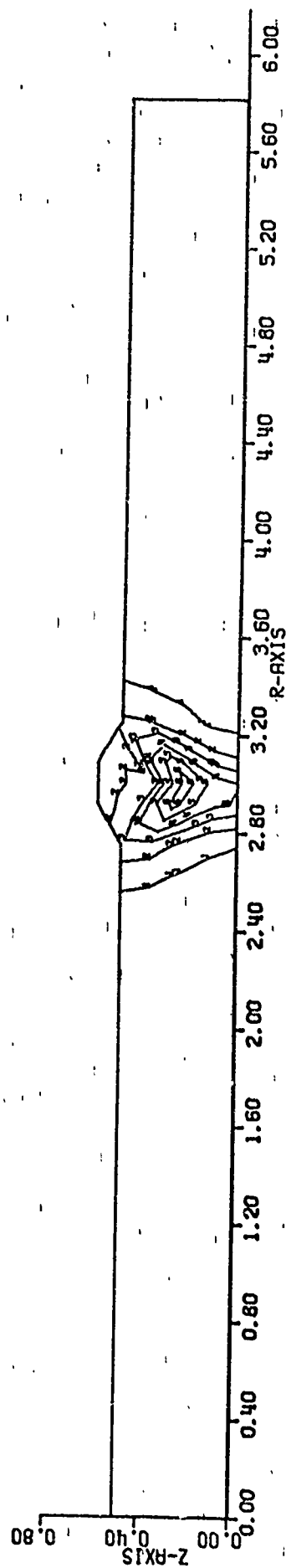
FIG. 16

1/2IN WELD.AS WELDED

EQUIV STRESS

C(1) = 1.22871117E+03
C(2) = 1.37839037E+04
C(3) = 2.63390963E+04
C(4) = 3.88942888E+04
C(5) = 5.14494814E+04
C(6) = 6.40046739E+04
C(7) = 7.65598665E+04
C(8) = 8.91150590E+04
C(9) = 1.01670252E+05
C(10) = 1.14225444E+05
C(11) = 1.26780637E+05
C(12) = 1.39335829E+05
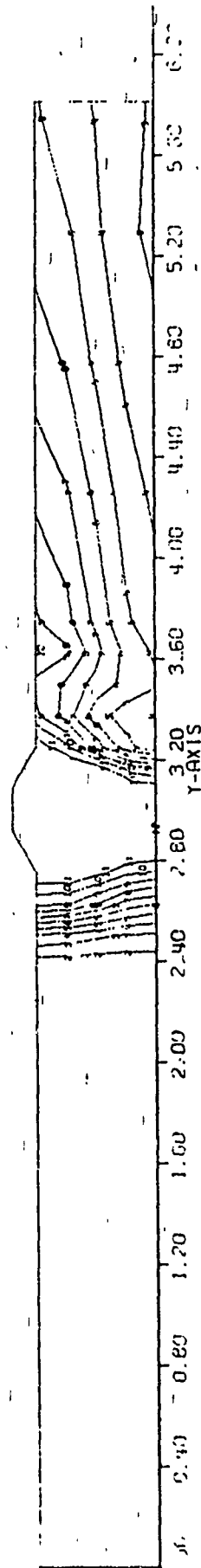
FIG. 17
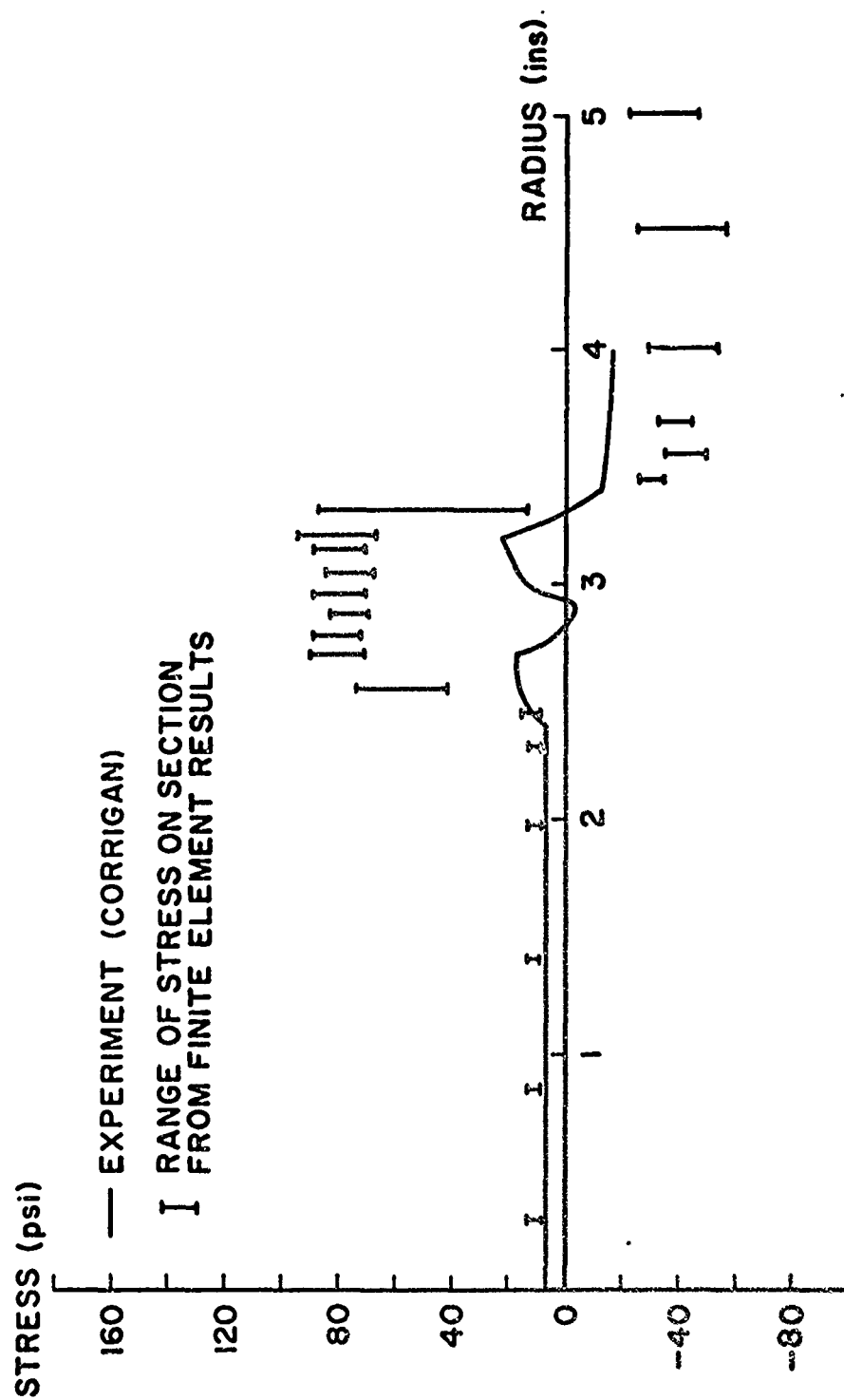
FIG. 18 TANGENTIAL STRESS, HY130/150 $\frac{1}{2}$" DISC AFTER 2HRS. 1000°F
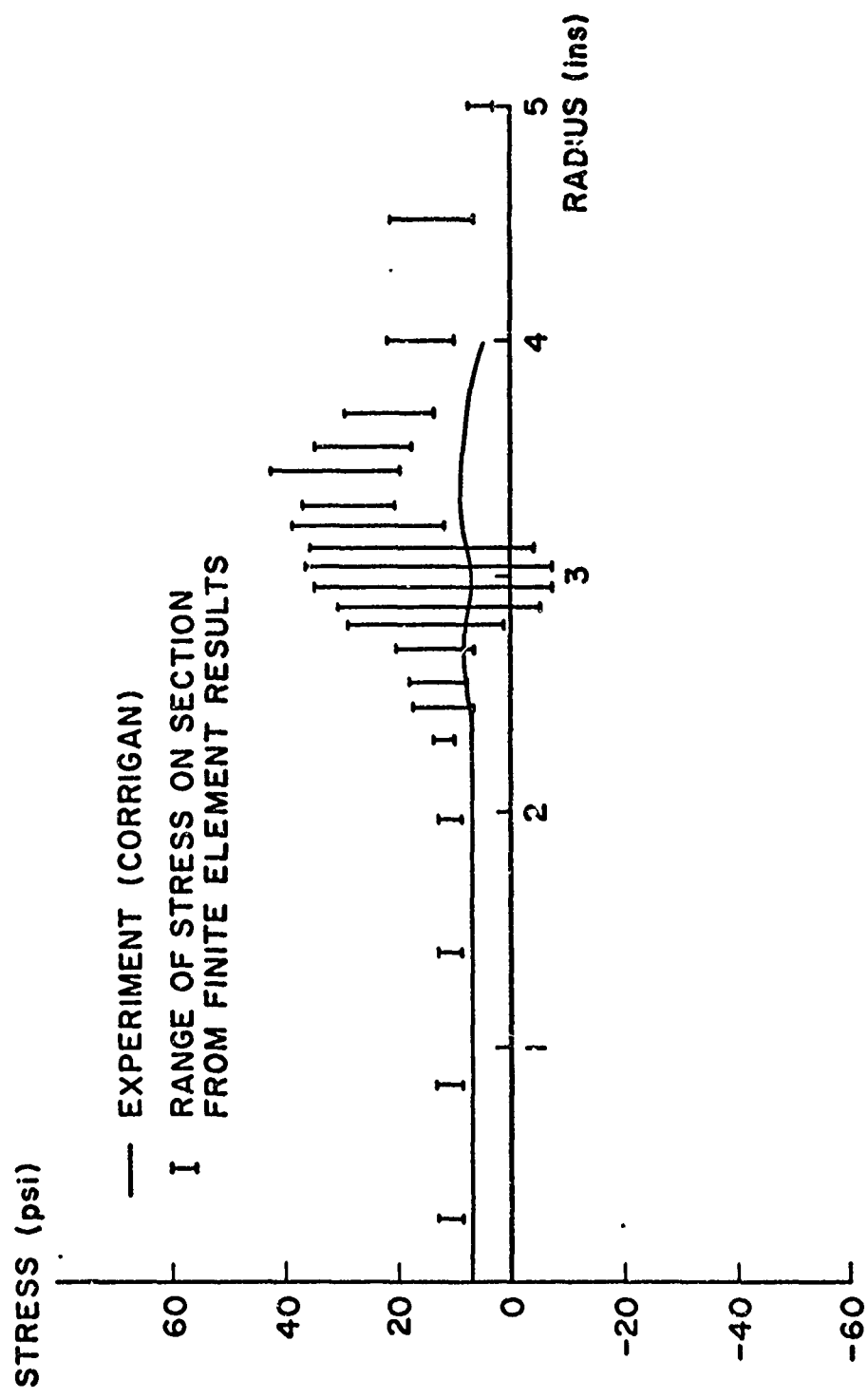
FIG. 19   RADIAL STRESS, HYI30/I50, ½" DISC, AFTER 2HRS. AT I000°F
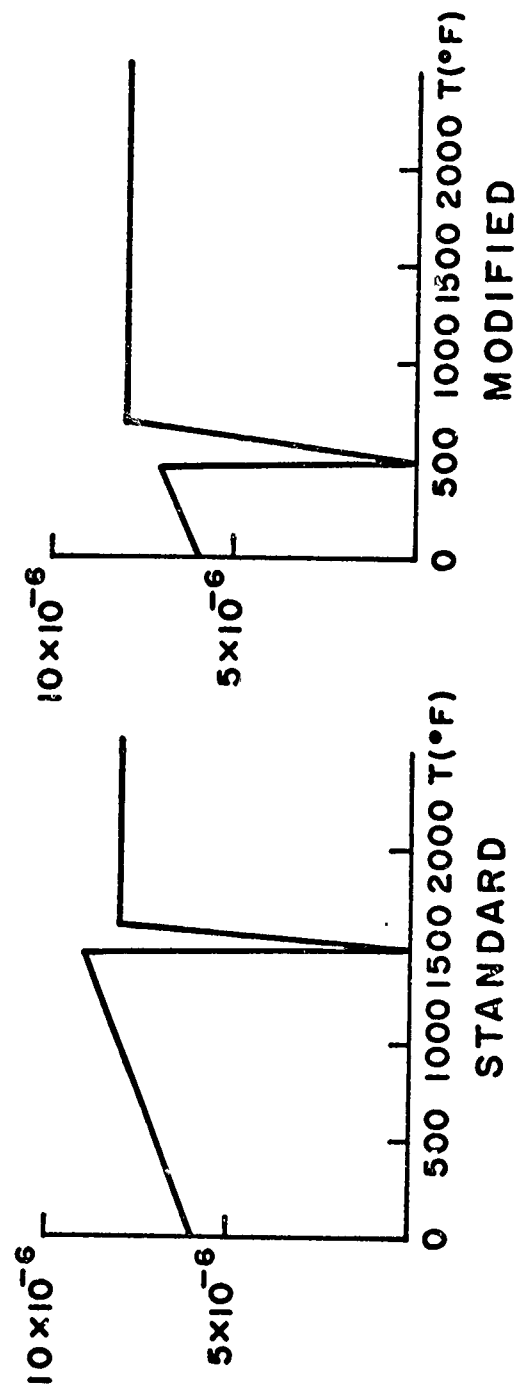
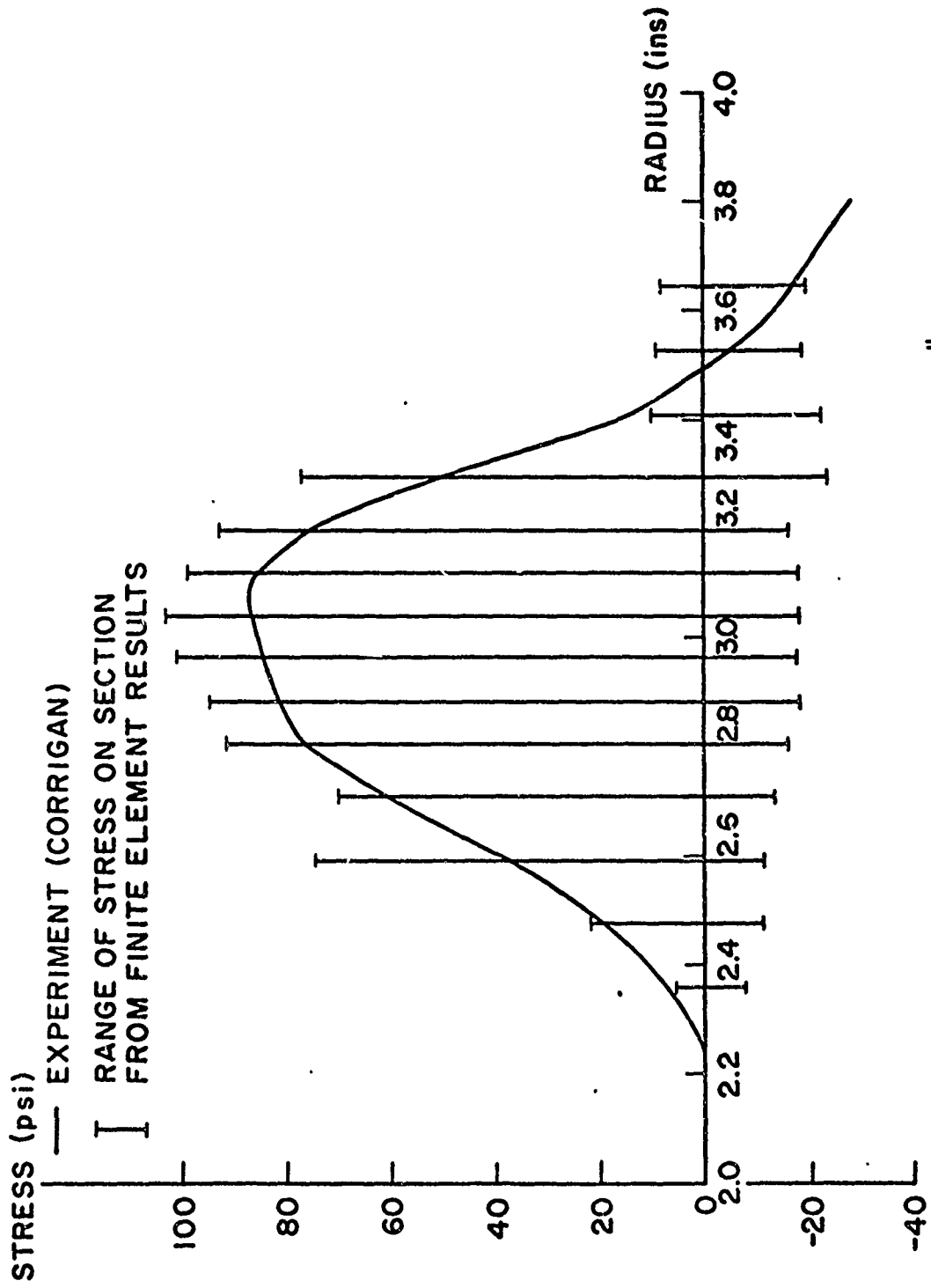FIG. 20 MODIFICATION OF THERMAL EXPANSION CURVES FOR LOW TEMPERATURE PHASE CHANGE
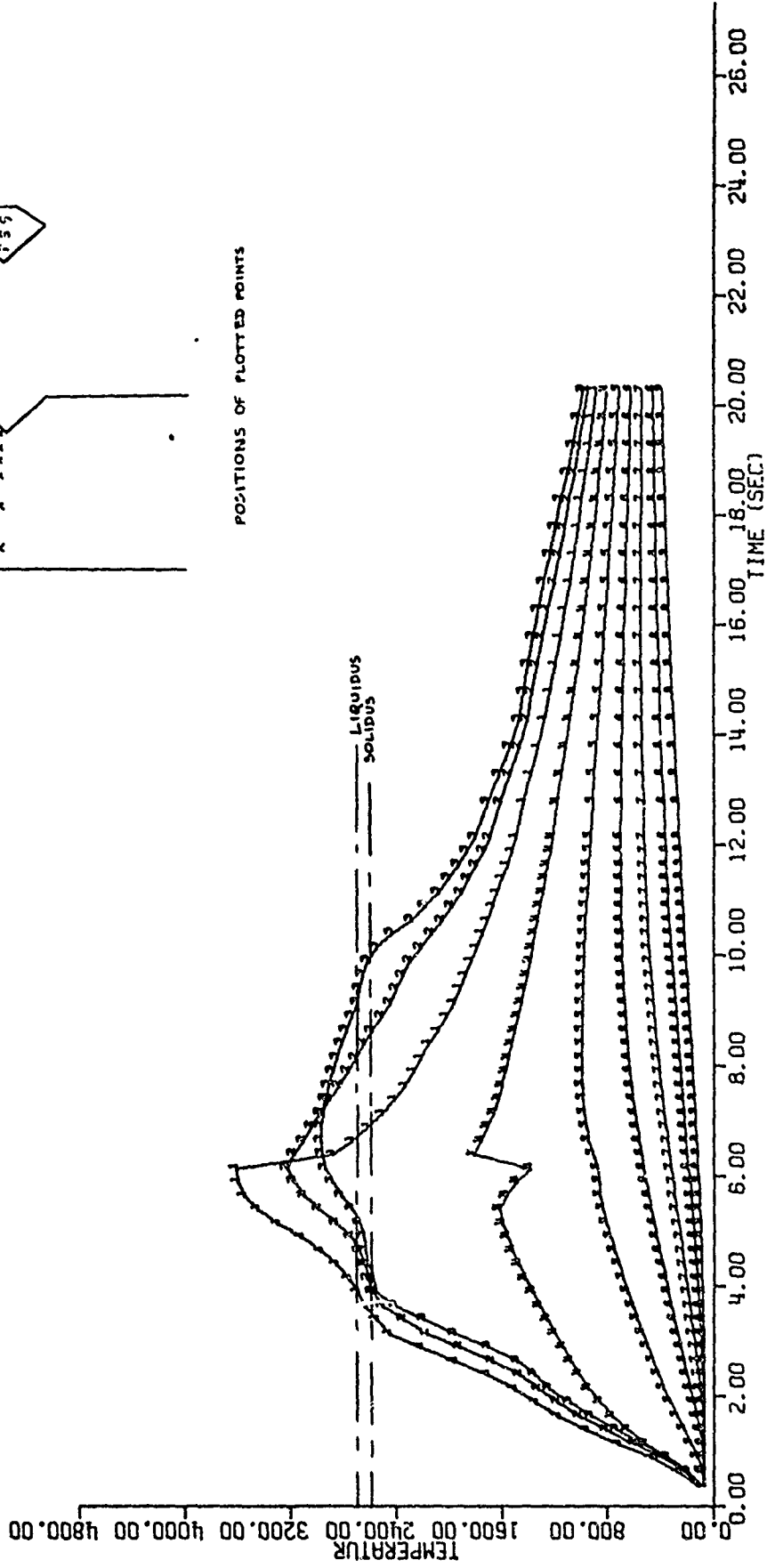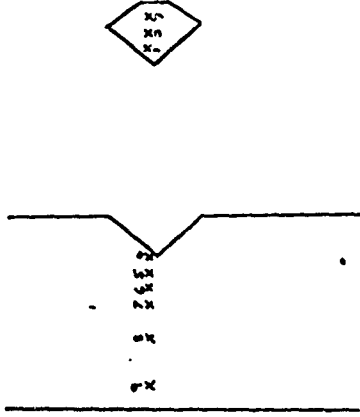
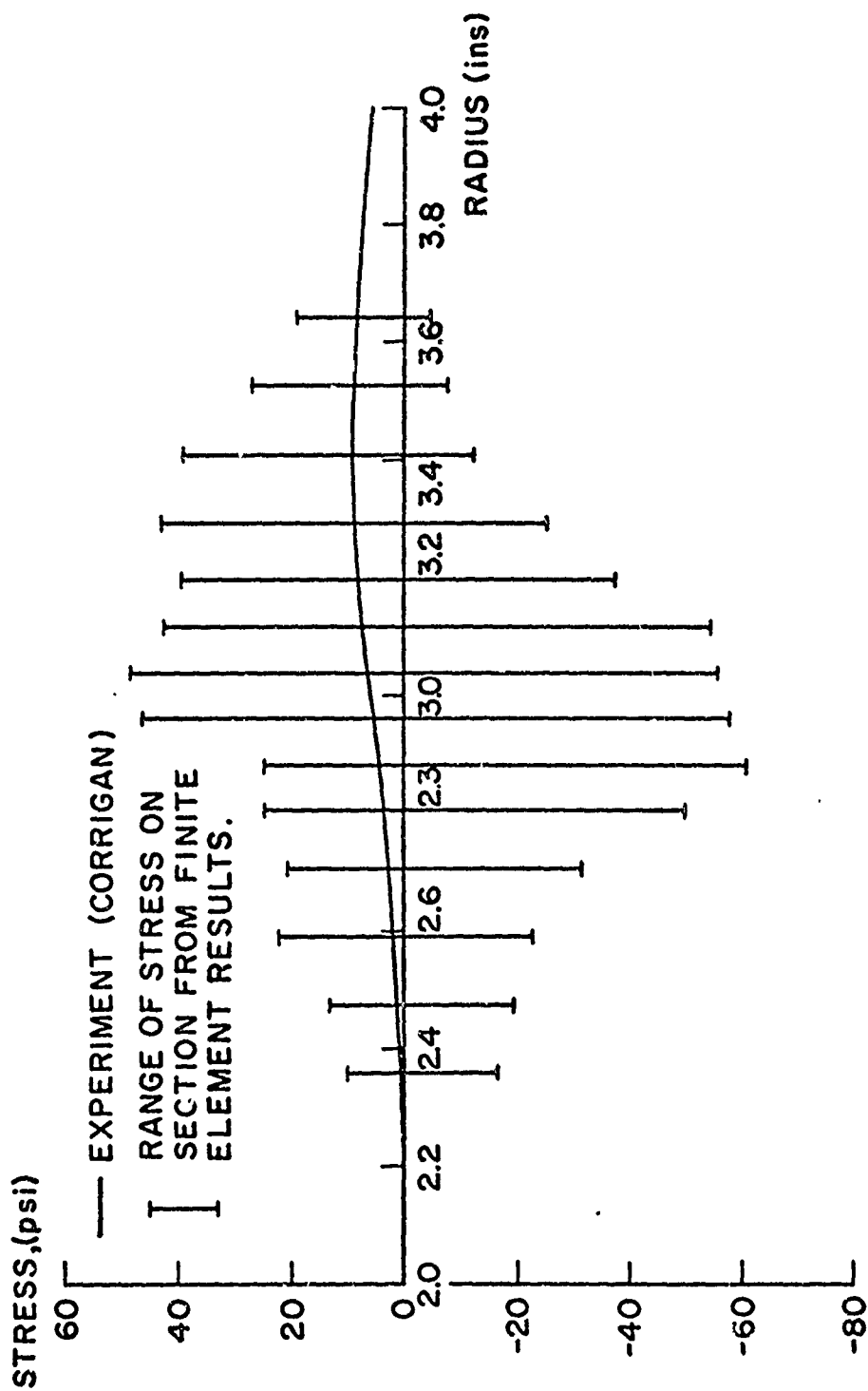FIG. 21

FIG. 22 AS WELDED TANGENTIAL STRESS, HY80, 1" DISC.

FIG. 23 AS WELDED RADIAL STRESS, HY80, 1" DISC.

1IN.DISC AS WELDED

EQUIV PLASTIC STRAI

C(1)=0.00238
C(2)=0.00713
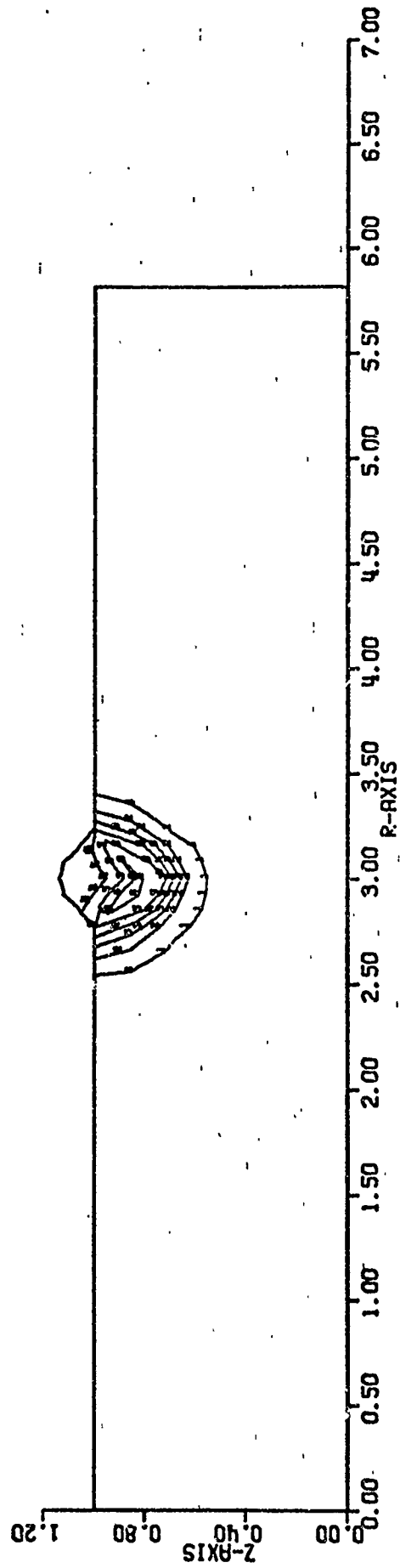C(3)=0.01189
C(4)=0.01664
C(5)=0.02140
C(6)=0.02616

FIG. 24